Mesoscale Biology

A Computational Scientist's Guide

Understanding Human Biology from Microns to Millimeters

Transport, Mechanics, and Mechanotransduction at the Tissue Scale

Sreekanth Pannala

January 29, 2026

Contents

Part I

Foundations of Mesoscale Biology

Chapter 1

Introduction to the Mesoscale

1.1 The Central Challenge: Bridging Scales in Living Systems

Biology has achieved remarkable success through reductionism—dissecting organisms into organs, tissues, cells, and molecules. The Human Genome Project catalogued our genetic blueprint; proteomics maps the protein machinery; metabolomics traces biochemical pathways. Yet this "parts list" approach fundamentally fails to predict emergent behaviors at the system level.

Principle 1.1 (The Mesoscale Gap)**.** *A critical knowledge gap exists at the* ***mesoscale****—the spatiotemporal regime spanning* $10\,\mu m$ *to* $10\,mm$ *in space and milliseconds to minutes in time. This is where:*

- *Stochastic molecular noise consolidates into deterministic tissue behavior*
- *Diffusion limits are overcome by advection*
- *Fluid forces reshape cellular architecture*
- *Physical forcing transduces into biological signals*

The mesoscale is the *theater of transport*—the liver lobule, intestinal villus, perivascular spaces of the brain, and the alveolar-capillary interface all operate in this regime. Here, the continuum hypothesis of fluid mechanics begins to interact with the discrete nature of cellular agents.

1.2 Defining the Mesoscale

1.2.1 Spatial Scales in Biology

Biological systems span an extraordinary range of scales:

Scale	**Range**	**Examples**
Molecular	$< 10\,\text{nm}$	Proteins, DNA, ion channels
Subcellular	10 nm – 1 μm	Organelles, cytoskeleton
Cellular	1 – 100 μm	Individual cells
Mesoscale	**10 μm – 10 mm**	**Villi, lobules, PVS**
Organ	1 cm – 10 cm	Heart, liver, brain
Organism	0.1 – 2 m	Whole body

1.2.2 Temporal Scales

Similarly, biological processes span many orders of magnitude in time:

Scale	Range	Examples
Molecular	fs – ns	Bond vibrations, electron transfer
Signaling	μs – ms	Ion channel gating, enzyme kinetics
Mesoscale	**ms – min**	**Transport, flow, mechanics**
Cellular	min – hours	Cell division, migration
Tissue	hours – days	Remodeling, adaptation
Organism	days – years	Development, aging

1.3 Key Dimensionless Numbers at the Mesoscale

The physics governing mesoscale biology can be characterized by several dimensionless numbers that reveal the dominant transport mechanisms.

1.3.1 Reynolds Number

The Reynolds number compares inertial to viscous forces:

$$\mathrm{Re} = \frac{\rho U L}{\mu} = \frac{U L}{\nu} \tag{1.1}$$

At the mesoscale, Re is typically very low (10^{-3} to 10^{2}), indicating that viscous forces dominate. This is the realm of **Stokes flow** where:

- Flow is laminar and reversible
- Inertia is negligible
- Boundary layers extend through the entire domain

Example 1.1 (Typical Reynolds Numbers)**.**

- *CSF in perivascular space:* $\mathrm{Re} \approx 10^{-3}$
- *Intestinal lumen flow:* $\mathrm{Re} \approx 1 - 10$
- *Arterial blood flow:* $\mathrm{Re} \approx 100 - 1000$
- *Blood flow in capillaries:* $\mathrm{Re} \approx 10^{-3}$

1.3.2 Peclet Number

The Peclet number compares advective to diffusive transport:

$$\mathrm{Pe} = \frac{U L}{D} \tag{1.2}$$

At the mesoscale, Pe is often *high* (10 to 10^{4}), meaning advection dominates diffusion. This is critical because:

- Diffusion alone is too slow for metabolic demands
- Flow organization becomes essential for transport
- Stagnant regions develop mass transfer limitations

Principle 1.2 (High Pe, Low Re)**.** *The mesoscale is uniquely characterized by the combination of low Reynolds number (viscous-dominated flow) and high Peclet number (advection-dominated transport). This combination makes flow organization critical for metabolic function.*

1.3.3 Womersley Number

The Womersley number characterizes pulsatile flow:

$$\mathrm{Wo} = R\sqrt{\frac{\omega}{\nu}} = R\sqrt{\frac{2\pi f}{\nu}} \tag{1.3}$$

where ω is the angular frequency and f is the frequency of pulsation.

- $\mathrm{Wo} < 1$: Quasi-steady flow; velocity profile is parabolic (Poiseuille)
- $\mathrm{Wo} > 10$: Highly pulsatile; plug flow with thin boundary layers
- $\mathrm{Wo} \sim 1$: Intermediate regime with complex profiles

1.3.4 Damköhler Number

The Damköhler number compares reaction rate to transport rate:

$$\mathrm{Da} = \frac{\tau_{\text{transport}}}{\tau_{\text{reaction}}} = \frac{kL}{U} \tag{1.4}$$

- $\mathrm{Da} \ll 1$: Reaction-limited; transport is fast, reaction is slow
- $\mathrm{Da} \gg 1$: Transport-limited; reaction is fast, transport is slow
- $\mathrm{Da} \sim 1$: Both processes are important

1.4 Why the Mesoscale Has Been Overlooked

Several factors have contributed to the historical neglect of mesoscale biology:

1.4.1 Experimental Challenges

- **Resolution gaps**: Optical microscopy reaches down to $\sim$0.2 μm; MRI resolves $\sim$0.5 mm. The mesoscale falls in between.
- **Dynamic measurement**: Tracking fast flows in complex geometries requires specialized techniques.
- **In vivo access**: Tissue architecture is disrupted by sectioning; live imaging is limited in depth.

1.4.2 Computational Challenges

- **Scale separation**: Molecular simulations (ns) cannot reach tissue times (s).
- **Heterogeneity**: Tissues are not homogeneous; effective medium theories fail.
- **Coupling**: Multiple physics (fluid, solid, chemical) interact nonlinearly.

1.4.3 Disciplinary Silos

- Biologists focus on molecular mechanisms
- Engineers focus on bulk transport
- Physicists focus on model systems
- The mesoscale falls between disciplines

1.5 The Role of Physical Forcing

A central thesis of this book is that **physical forcing** is not a perturbation to be ignored but a fundamental feature of biological design.

1.5.1 Intrinsic Physical Forcing

Biological systems generate continuous mechanical perturbations:

Source	Frequency	System
Cardiac pulsation	∼1 Hz	Vascular, glymphatic
Respiration	∼0.2 Hz	Pulmonary, CSF
Peristalsis	∼0.05 Hz	Gastrointestinal
Ciliary beating	∼10 Hz	Respiratory, reproductive
Vasomotion	∼0.1 Hz	Microcirculation

1.5.2 Physical Forcing Enhances Transport

Evidence suggests that pulsatile flow and mechanical vibration significantly enhance mass transfer:

- **Boundary layer disruption**: Oscillatory flow prevents stagnant layers
- **Taylor dispersion**: Pulsation enhances effective diffusivity
- **Mixing enhancement**: Up to 50% improvement in spacer-filled channels

Principle 1.3 (Physical Forcing Enhancement)**.** *Pulsatile flow and mechanical vibration enhance mass transfer by 30–50% through boundary layer disruption and mixing. This is not noise to be filtered but a design feature evolved for transport optimization.*

1.6 Examples of Mesoscale Biological Systems

1.6.1 The Intestinal Villus

The small intestine is lined with finger-like projections called villi:

- **Dimensions**: 0.5–1.5 mm tall, ∼0.1 mm diameter
- **Function**: Increase surface area for nutrient absorption
- **Challenge**: Maintain nutrient gradients in flowing chyme
- **Physical forcing**: Peristaltic contractions at ∼0.05 Hz

1.6.2 The Liver Lobule

The functional unit of the liver is the lobule:

- **Dimensions**: ∼1–2 mm diameter
- **Function**: Metabolize blood from portal vein and hepatic artery
- **Challenge**: Create oxygen and metabolite gradients for zonation
- **Physical forcing**: Pulsatile arterial flow

1.6.3 The Perivascular Space (Glymphatic)

The brain's waste clearance system operates in perivascular spaces:

- **Dimensions**: 20–100 μm wide channels around vessels
- **Function**: Clear metabolic waste including amyloid-β
- **Challenge**: Drive flow against low permeability
- **Physical forcing**: Arterial pulsation at cardiac frequency

1.6.4 The Alveolar-Capillary Interface

Gas exchange in the lung occurs at the mesoscale:

- **Dimensions**: Alveoli $\sim$200 μm; capillaries $\sim$8 μm
- **Function**: O_2/CO_2 exchange between air and blood
- **Challenge**: Maximize surface area while minimizing diffusion distance
- **Physical forcing**: Respiratory cycling at $\sim$0.2 Hz

1.7 The Computational Framework Approach

To address the mesoscale gap, we need computational frameworks that:

1. **Couple multiple physics**: Fluid dynamics, mass transport, solid mechanics, biochemistry
2. **Handle multiple scales**: Molecular signaling, cellular agents, tissue continuum
3. **Include physical forcing**: Pulsatility, vibration, deformation
4. **Validate against experiments**: Organ-on-chip, clinical imaging

The MesoBio framework, described throughout this book, implements this approach using:

- Lattice Boltzmann methods for fluid dynamics
- Agent-based models for cells
- Immersed boundary methods for FSI
- GPU acceleration for computational efficiency

1.8 Summary

Key Concepts

- The **mesoscale** spans 10 μm to 10 mm spatially and ms to min temporally
- It is characterized by **low Re** (viscous-dominated) and **high Pe** (advection-dominated)
- **Physical forcing** (pulsation, peristalsis) is essential, not incidental

- The mesoscale has been **historically neglected** due to experimental and disciplinary barriers
- Understanding the mesoscale is key to **transport-related diseases**

1.9 Further Reading

1. Wittkowski, R. et al. (2023). "Mesoscale simulations: An indispensable approach to understand biomembranes." *Biophysical Journal*.
2. Quarteroni, A. et al. (2017). "Multiscale and multiphysics modeling in cardiovascular physiology." *J Computational Physics*.
3. Swartz, M.A. & Fleury, M.E. (2007). "Interstitial flow and its effects in soft tissues." *Annual Review of Biomedical Engineering*.

Chapter 2

Thermodynamics of Living Systems

2.1 Schrödinger's Question: What is Life?

In 1944, physicist Erwin Schrödinger posed the fundamental question in his Dublin lectures, later published as *What is Life?* His insights, remarkably prescient before DNA's discovery, identified two pillars of living systems.

2.1.1 The Aperiodic Crystal

Schrödinger proposed that hereditary information must be stored in an "aperiodic crystal"—a structure with specific but non-periodic atomic arrangement:

> *"The chromosome structures are at the same time instrumental in bringing about the development they foreshadow. They are law-code and executive power—or, to use another simile, they are architect's plan and builder's craft—in one."* —Schrödinger, 1944

This vision directly inspired Watson and Crick. DNA is precisely an aperiodic solid: the sequence of bases (A, T, G, C) encodes information through its specific non-repeating pattern.

2.1.2 Negentropy: Order Against the Second Law

Schrödinger introduced the concept of **negentropy**—the entropy an organism exports to maintain internal order:

$$\frac{dS_{\text{internal}}}{dt} = \dot{S}_{\text{production}} - \dot{S}_{\text{export}} < 0 \quad \text{(locally)} \tag{2.1}$$

Living systems maintain low internal entropy by consuming free energy and exporting high-entropy waste. This is not a violation of thermodynamics but its exploitation—life *surfs the gradient* between high-quality energy sources and low-temperature sinks.

2.2 Non-Equilibrium Thermodynamics

Living systems operate far from equilibrium, continuously dissipating free energy to maintain organization.

2.2.1 Entropy Production Rate

For a continuous system with multiple irreversible processes, the entropy production rate σ is given by:

$$\sigma = \sum_i J_i X_i \geq 0 \tag{2.2}$$

where J_i are thermodynamic **fluxes** and X_i are conjugate **forces**:

Process	**Flux** J	**Force** X
Heat conduction	$\mathbf{q}$ (heat flow)	$\nabla(1/T)$
Mass diffusion	$\mathbf{J}_k$ (species flux)	$-\nabla(\mu_k/T)$
Chemical reaction	ξ (extent)	A/T (affinity)
Viscous flow	$\boldsymbol{\Pi}$ (stress)	$\nabla\mathbf{v}/T$

2.2.2 Linear Phenomenological Laws

Near equilibrium, fluxes are linear functions of forces:

$$J_i = \sum_j L_{ij} X_j \tag{2.3}$$

where L_{ij} are the Onsager coefficients satisfying the reciprocal relations:

$$L_{ij} = L_{ji} \tag{2.4}$$

This symmetry reflects microscopic reversibility and has profound consequences for coupled transport processes.

2.2.3 Minimum Entropy Production Principle

Prigogine showed that for systems near equilibrium with fixed boundary conditions, steady states minimize total entropy production:

$$\frac{\partial}{\partial t} \int_V \sigma \, dV = 0 \quad \text{at steady state} \tag{2.5}$$

This principle provides a variational framework for predicting transport network architecture.

Principle 2.1 (Entropy Production Minimization)**.** *Biological transport networks evolve to minimize dissipation while meeting metabolic demand. Vessels branch and organize to reduce the total entropy production rate.*

2.3 Nick Lane and the Proton-Motive Force

Building on Schrödinger's thermodynamic insight, biochemist Nick Lane has illuminated how life harnesses energy through **chemiosmotic coupling**.

2.3.1 The Alkaline Vent Hypothesis

Lane proposes that life originated at alkaline hydrothermal vents where natural proton gradients existed:

- Alkaline vent fluids (pH $\sim$ 9–11) meet acidic ocean water (pH $\sim$ 5–6)
- This creates a ΔpH $\sim$ 3–5 units across porous FeS/NiS barriers
- The gradient drives reduction of CO_2 by H_2, producing organic molecules

2.3.2 The Proton-Motive Force

The proton-motive force (Δp) combines chemical and electrical gradients:

$$\Delta p = \Delta\psi - \frac{2.303RT}{F}\Delta\text{pH} \tag{2.6}$$

Typical values in mitochondria:

- $\Delta\psi \approx 150$ mV (membrane potential)
- $\Delta\text{pH} \approx 0.5$ units
- Total $\Delta p \approx 180$ mV

2.3.3 ATP Synthesis

The proton gradient drives ATP synthase, a rotary molecular motor:

$$\text{ADP} + \text{P}_i + n\text{H}^+_{\text{out}} \rightarrow \text{ATP} + n\text{H}^+_{\text{in}} \tag{2.7}$$

where $n \approx 3$–4 protons per ATP. The free energy yield:

$$\Delta G_{\text{ATP}} = \Delta G^0 + RT \ln \frac{[\text{ATP}]}{[\text{ADP}][\text{P}_i]} \approx -50 \text{ kJ/mol} \tag{2.8}$$

2.4 Mitochondria: The Eukaryotic Breakthrough

Lane argues that the endosymbiotic acquisition of mitochondria was the singular event enabling eukaryotic complexity.

2.4.1 The Surface-Area Problem

ATP synthesis occurs at membranes, but genes must be proximal to control it:

- Cell volume grows as r^3
- Membrane area grows as r^2
- Large cells cannot maintain sufficient ATP synthesis per unit volume

2.4.2 The Mitochondrial Solution

Mitochondria solve this by internalizing vast membrane surface area:

- A human cell contains $\sim$1000 mitochondria
- Total cristae membrane area $\sim$14,000 μm^2
- This is orders of magnitude more than the plasma membrane
- Enables the energy budget for large genomes and complex multicellularity

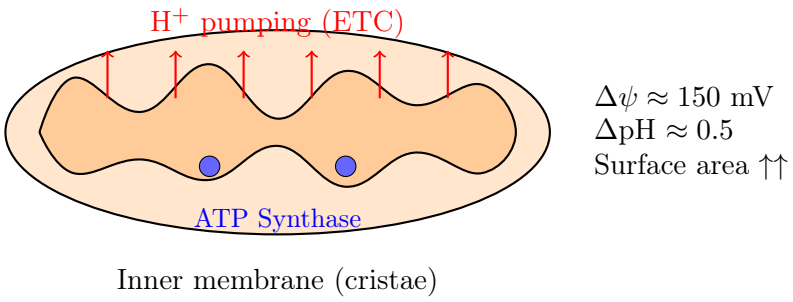

Figure 2.1: Mitochondrial cristae maximize membrane surface area for ATP synthesis. The proton gradient (Δp) drives ATP synthase rotation.

2.5 Six Pillars of Life

Building on Schrödinger and Lane, we identify six fundamental characteristics that any computational framework must address:

1. **Information (Genetic Code)**: Encoded in aperiodic DNA sequences, encapsulating 4 billion years of evolutionary exploration
2. **Energy Flows**: Sustained within thermodynamic constraints via chemiosmotic coupling, maintaining ΔG gradients far from equilibrium
3. **Ambient Temperature Operation**: Reactions at ∼300 K impose kinetic constraints—enzymes achieve rate enhancements of 10^{10}–10^{17} through transition state stabilization
4. **Sustainability**: Resource-constrained existence (except solar energy input); local recycling via decomposition; closed material loops
5. **Modular Architecture**: Built on time-tested modules through symbiosis (mitochondria, chloroplasts, microbiome); hierarchical organization
6. **Atomistic Efficiency**: Precise electron and proton channeling; near-unity quantum yields in photosynthesis; minimal dissipation in molecular motors

2.6 Non-Equilibrium Steady States in Biology

2.6.1 NESS vs. Equilibrium

Living systems maintain non-equilibrium steady states (NESS):

	Equilibrium	**NESS**
Energy input	None	Continuous
Entropy production	Zero	Positive, constant
Free energy	Minimum	Above minimum
Fluxes	Zero	Non-zero, balanced
Examples	Dead tissue	Living cell

2.6.2 Maintaining NESS

The energetic cost of maintaining a NESS can be estimated from entropy production:

$$\dot{W}_{\text{min}} = T \int_V \sigma \, dV \tag{2.9}$$

Recent theoretical advances allow estimation of entropy production from partial measurements of biological trajectories, even when some degrees of freedom are hidden.

2.7 Thermodynamic Constraints on Transport

2.7.1 Efficiency Limits

Thermodynamics places fundamental limits on biological transport efficiency. For a molecular motor operating between states:

$$\eta = \frac{W_{\text{useful}}}{\Delta G_{\text{input}}} \leq 1 - \frac{T\Delta S_{\text{produced}}}{\Delta G_{\text{input}}} \tag{2.10}$$

2.7.2 Trade-offs

Living systems face fundamental trade-offs:

- **Speed vs. efficiency**: Faster processes dissipate more
- **Precision vs. cost**: Error correction requires energy
- **Robustness vs. responsiveness**: Stability requires energy investment

2.8 Summary

Key Concepts

- Life maintains **low internal entropy** by exporting entropy to the environment
- **Chemiosmotic coupling** (proton gradients) powers most biological energy conversion
- **Mitochondria** solved the surface-area problem, enabling complex eukaryotes
- Living systems exist in **non-equilibrium steady states**, continuously dissipating free energy
- **Entropy production minimization** provides a design principle for transport networks

2.9 Further Reading

1. Schrödinger, E. (1944). *What is Life?* Cambridge University Press.
2. Lane, N. (2015). *The Vital Question.* W.W. Norton.
3. Prigogine, I. (1980). *From Being to Becoming.* W.H. Freeman.
4. England, J.L. (2015). "Dissipative adaptation in driven self-assembly." *Nature Nanotechnology.*

Chapter 3

Information Theory in Biology

3.1 Information as a Biological Quantity

Biological systems are unique in that they *process information*. From gene regulation to neural computation, cells encode, transmit, and decode signals. Information theory, developed by Claude Shannon for communication systems, provides a rigorous framework for quantifying these processes.

3.2 Shannon Information Theory

3.2.1 Entropy as Uncertainty

The Shannon entropy of a discrete random variable X with probability distribution $p(x)$ is:

$$H(X) = -\sum_{x} p(x) \log_2 p(x) \quad \text{[bits]} \tag{3.1}$$

This measures the **uncertainty** or **information content** of the variable.

Example 3.1 (Entropy Examples).

- *Fair coin:* $H = -2 \times 0.5 \log_2(0.5) = 1$ *bit*
- *Biased coin (90/10):* $H = -0.9 \log_2(0.9) - 0.1 \log_2(0.1) = 0.47$ *bits*
- *Certain outcome:* $H = 0$ *bits*

3.2.2 Mutual Information

For two random variables X (input) and Y (output), the mutual information measures how much knowing Y tells us about X:

$$I(X;Y) = H(Y) - H(Y|X) = H(X) - H(X|Y) \tag{3.2}$$

This is the **reduction in uncertainty** about X after observing Y.

3.2.3 Channel Capacity

The channel capacity C is the maximum mutual information over all input distributions:

$$C = \max_{p(x)} I(X;Y) \tag{3.3}$$

This represents the maximum rate at which information can be reliably transmitted through a noisy channel.

3.3 Information Processing in Cells

3.3.1 Gene Regulatory Networks

Gene expression can be viewed as an information channel:

- **Input**: Transcription factor concentration
- **Channel**: Promoter binding, transcription, translation
- **Output**: Protein concentration
- **Noise**: Stochastic gene expression

Measurements show that a single gene promoter typically transmits ∼1–2 bits of information about transcription factor levels.

3.3.2 Signaling Pathways

Signal transduction pathways also have limited channel capacity:

Pathway	Capacity (bits)	Interpretation
MAPK cascade	1–2	Binary on/off
NF-κB	1–1.5	Graded response
p53 (oscillations)	2–3	Multiple levels
YAP/TAZ	1–2	Stiffness sensing

Principle 3.1 (Limited Channel Capacity)**.** *Most biological signaling pathways have a channel capacity of 1–2 bits, meaning cells can reliably distinguish only 2–4 discrete input levels. This "digital" processing emerges from biochemical noise constraints.*

3.4 Mechanotransduction Information

3.4.1 Channel Capacity of Mechanical Sensing

For mechanotransduction via the YAP/TAZ pathway:

- **Input** X: Substrate stiffness or mechanical strain
- **Output** Y: Nuclear/cytoplasmic YAP ratio
- **Channel**: Focal adhesions $\rightarrow$ cytoskeleton $\rightarrow$ YAP localization

The estimated channel capacity is $C \approx 1$–2 bits, meaning cells can distinguish roughly 2–4 discrete stiffness levels (e.g., soft, medium, stiff, very stiff).

3.4.2 Implications for Tissue Engineering

The limited information capacity of mechanotransduction has implications:

- Cells cannot sense stiffness with arbitrary precision
- Gradients must span distinguishable levels
- Temporal modulation may increase effective capacity

3.5 The Genetic Code as Information

3.5.1 Information Content of DNA

The human genome contains approximately:

$$\text{Information} = 3 \times 10^9 \text{ bp} \times 2 \text{ bits/bp} = 6 \times 10^9 \text{ bits} \approx 750 \text{ MB} \tag{3.4}$$

However, the *functional* information is much less due to:

- Non-coding regions (∼98% of genome)
- Redundancy in the genetic code
- Repetitive sequences

3.5.2 Error Correction in Replication

DNA replication achieves error rates of $\sim 10^{-10}$ per base pair through:

- Polymerase selectivity ($\sim 10^{-4}$)
- Proofreading exonuclease ($\sim 10^{-2}$)
- Mismatch repair ($\sim 10^{-3}$)

This error correction has an energetic cost, consistent with the thermodynamic bound:

$$\text{Energy per bit} \geq k_B T \ln 2 \approx 0.7 k_B T \tag{3.5}$$

3.6 Kolmogorov Complexity

Beyond Shannon information, we consider **Kolmogorov complexity**—the length of the shortest program that produces a given output.

3.6.1 Definition

The Kolmogorov complexity $K(x)$ of a string x is:

$$K(x) = \min\{|p| : U(p) = x\} \tag{3.6}$$

where U is a universal Turing machine and $|p|$ is the length of program p.

3.6.2 Applications in Biology

- **Morphogenesis**: The developmental "program" that transforms a fertilized egg into an organism has high complexity, but the genome is remarkably compressed
- **Evolution**: Natural selection explores the space of possible genomes, guided by fitness but constrained by complexity
- **Self-organization**: Many biological patterns (branching, spirals) have low Kolmogorov complexity—they can be generated by simple rules

3.7 Information Flow at the Mesoscale

3.7.1 Spatial Information Processing

At the mesoscale, information is processed spatially:

System	Input	Spatial Processing
Liver lobule	Blood composition	Zonation (periportal vs. central)
Intestinal crypt	Wnt gradient	Stem cell niche localization
Tumor	O_2 gradient	Hypoxic core differentiation

3.7.2 Temporal Information Processing

Pulsatile signals can encode more information than steady-state:

- **Frequency modulation**: Different frequencies encode different signals
- **Duration encoding**: Pulse width carries information
- **Phase relationships**: Relative timing between signals

Example 3.2 (p53 Oscillations)**.** *The tumor suppressor p53 exhibits oscillations in response to DNA damage. The number of pulses (not amplitude) encodes the extent of damage and determines cell fate (repair vs. apoptosis). This increases effective channel capacity beyond a simple steady-state response.*

3.8 The Cell as a Computational Entity

3.8.1 Decision Making

Cells make decisions based on environmental cues:

- Proliferate or quiesce?
- Migrate or stay?
- Differentiate or maintain stemness?
- Survive or undergo apoptosis?

These decisions integrate multiple input signals with limited channel capacity, suggesting cellular computation is fundamentally "digital" (threshold-based) rather than analog.

3.8.2 Algorithmic Probability

Cells may implement something akin to Bayesian inference:

$$P(\text{state}|\text{signals}) \propto P(\text{signals}|\text{state}) \times P(\text{state}) \tag{3.7}$$

The "prior" $P(\text{state})$ is encoded in network architecture and epigenetic state.

3.9 Information-Theoretic Bounds in Biology

3.9.1 Speed-Accuracy Trade-off

There is a fundamental trade-off between speed and accuracy in biochemical sensing:

$$\text{Error rate} \times \text{Time} \geq \frac{1}{4Dc} \tag{3.8}$$

where D is diffusion coefficient and c is concentration. Faster sensing requires more energy to overcome this bound.

3.9.2 Kinetic Proofreading

Hopfield's kinetic proofreading shows how energy dissipation can enhance specificity beyond equilibrium limits:

$$\text{Specificity}_{\text{kinetic}} = \left(\text{Specificity}_{\text{equilibrium}}\right)^{n} \tag{3.9}$$

where n is the number of proofreading steps, each consuming $\sim k_B T$.

3.10 Summary

Key Concepts

- **Shannon entropy** quantifies uncertainty/information in biological signals
- **Channel capacity** of signaling pathways is typically 1–2 bits
- **Kolmogorov complexity** measures the "program length" of biological structures
- **Temporal encoding** (oscillations, pulses) increases effective channel capacity
- Cells are **computational entities** with fundamental information-processing constraints

3.11 Further Reading

1. Cover, T.M. & Thomas, J.A. (2006). *Elements of Information Theory*. Wiley.
2. Tkacik, G. & Bialek, W. (2016). "Information processing in living systems." *Annual Review of Condensed Matter Physics*.
3. Cheong, R. et al. (2011). "Information transduction capacity of noisy biochemical signaling networks." *Science*.

Chapter 4

The Constructal Law and Transport Networks

4.1 The Constructal Law

Adrian Bejan's **Constructal Law** provides a deterministic principle for the emergence of design in nature:

Principle 4.1 (Constructal Law)**.** *"For a finite-size flow system to persist in time (to live), its configuration must evolve such that it provides easier access to the currents that flow through it." —Bejan, 1996*

This is not a metaphor but a physical law: systems that survive are those that have evolved better flow architectures. The Constructal Law has been applied to:

- River drainage basins
- Vascular networks in biology
- Bronchial trees
- Urban street networks
- Electronic cooling systems

4.2 Murray's Law: Optimal Vascular Branching

4.2.1 Derivation

Consider a blood vessel of radius r and length L carrying flow rate Q. The total power required includes:

1. **Pumping power** (Poiseuille flow):
$$W_{\text{pump}} = Q\Delta P = \frac{8\mu L Q^2}{\pi r^4} \tag{4.1}$$
2. **Metabolic cost** of maintaining blood volume:
$$W_{\text{metabolic}} = b \cdot V = b \cdot \pi r^2 L \tag{4.2}$$
where b is the metabolic cost per unit volume.

Total power:
$$W_{\text{total}} = \frac{8\mu L Q^2}{\pi r^4} + b\pi r^2 L \tag{4.3}$$

4.2.2 Optimization

Minimizing W_{total} with respect to r at fixed Q:

$$\frac{\partial W_{\text{total}}}{\partial r} = -\frac{32\mu L Q^2}{\pi r^5} + 2b\pi r L = 0 \tag{4.4}$$

This gives $Q \propto r^3$, or equivalently:

$$\boxed{r_0^3 = r_1^3 + r_2^3} \tag{4.5}$$

This is **Murray's Law**: at a bifurcation, the cube of the parent vessel radius equals the sum of the cubes of daughter radii.

4.2.3 Consequences

For a symmetric bifurcation ($r_1 = r_2 = r_d$):

$$\frac{r_d}{r_0} = 2^{-1/3} \approx 0.794 \tag{4.6}$$

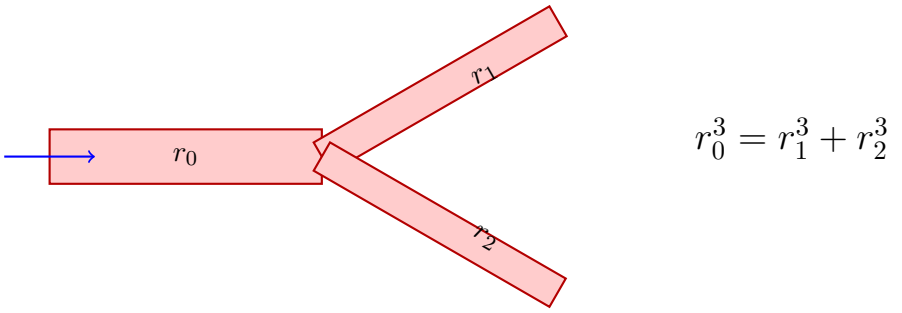

Figure 4.1: Murray's Law optimizes vascular branching by minimizing total power expenditure.

4.3 Allometric Scaling Laws

4.3.1 Metabolic Rate Scaling

Across species spanning many orders of magnitude in body mass, metabolic rate B scales as:

$$B \propto M^{3/4} \tag{4.7}$$

This 3/4 power law (Kleiber's Law) emerges from optimizing hierarchical transport networks that must service a 3D volume through a branching tree structure.

4.3.2 Derivation from Constructal Theory

Consider a fractal-like vascular network serving a body of mass M:

- Volume scales as $V \propto M$
- Linear dimension scales as $L \propto M^{1/3}$
- Optimal networks have n branching levels with $n \propto \log M$
- Each level reduces vessel size by factor $2^{-1/3}$ (Murray)

- Metabolic rate limited by terminal exchange area

The network optimization yields:

$$B = B_0 M^{3/4} \tag{4.8}$$

where $B_0 \approx 70$ W/kg$^{3/4}$ for mammals.

4.3.3 Other Allometric Relations

Quantity	Scaling	Origin
Metabolic rate	$M^{3/4}$	Network optimization
Heart rate	$M^{-1/4}$	$= B/$(stroke volume)
Lifespan	$M^{1/4}$	Total heartbeats constant
Aorta radius	$M^{3/8}$	Murray's Law + $B^{3/4}$
Capillary density	$M^{-1/4}$	Terminal exchange

4.4 Constructal Design in Specific Organs

4.4.1 The Lung

The bronchial tree optimizes gas exchange:

- 23 generations of branching
- First 16 generations: conducting airways (no exchange)
- Last 7 generations: respiratory zone (alveoli)
- Total surface area $\sim$70 m^2
- Diffusion distance $<$1 μm

The design balances:

- Minimizing dead space (conducting airways)
- Maximizing exchange area
- Minimizing pumping work

4.4.2 The Liver

The liver lobule architecture follows constructal principles:

- Hexagonal arrangement minimizes path length
- Dual blood supply (portal vein + hepatic artery)
- Central drainage (hepatic vein)
- Creates metabolic zonation

4.4.3 The Kidney

Renal architecture demonstrates multi-scale optimization:

- ∼1 million nephrons per kidney
- Countercurrent multiplier in loop of Henle
- Glomerular filtration followed by selective reabsorption
- Vasa recta maintain medullary gradient

4.5 Evolution of Flow Systems

4.5.1 Constructal Evolution

The Constructal Law predicts that flow systems *evolve* toward configurations with greater access:

$$\frac{d(\text{Access})}{dt} > 0 \tag{4.9}$$

This is not Darwinian evolution (no reproduction/selection) but physical evolution driven by thermodynamic forcing.

4.5.2 Time Scales of Constructal Evolution

System	Time Scale	Mechanism
River network	10^4–10^6 years	Erosion
Vascular remodeling	days–weeks	Angiogenesis/regression
Bronchial tree	developmental	Branching morphogenesis
Traffic network	years–decades	Planning/emergence

4.6 Angiogenesis and Network Evolution

4.6.1 Oxygen-Driven Angiogenesis

Tumor angiogenesis follows constructal principles:

1. Hypoxic cells secrete VEGF
2. VEGF gradient guides endothelial sprouting
3. New vessels increase oxygen access
4. Network remodels toward efficiency

4.6.2 Computational Modeling

The MesoBio framework implements angiogenesis modeling:

- Agent-based tip cells follow chemotactic gradients
- Stalk cells proliferate and form vessel tubes
- Flow computation determines perfused vs. pruned vessels
- Network evolves toward Murray's Law

4.7 Thermodynamic-Constructal Coupling

4.7.1 Entropy Production in Networks

For a vascular network, the total entropy production rate is:

$$\dot{S} = \sum_{\text{vessels}} \frac{Q_i \Delta P_i}{T} \tag{4.10}$$

At steady state with fixed metabolic demand, the network that minimizes $\dot{S}$ is the optimal design.

4.7.2 Constructal Optimization

The Constructal Law can be recast as:

$$\text{Minimize: } \int_V \sigma \, dV \quad \text{Subject to: } Q_{\text{total}} = Q_{\text{metabolic}} \tag{4.11}$$

This variational principle generates Murray's Law and other biological design rules.

4.8 Applications to Disease

4.8.1 Atherosclerosis

Atherosclerosis preferentially develops at branching points where:

- Local shear stress is disturbed
- Flow deviates from optimal (Murray) configuration
- Endothelial dysfunction occurs

4.8.2 Tumor Vasculature

Tumor vessels are notoriously disorganized:

- Violate Murray's Law
- High resistance, poor perfusion
- Heterogeneous oxygenation
- Creates therapeutic resistance

4.8.3 Glymphatic Dysfunction

Aging and disease reduce glymphatic efficiency:

- Arterial stiffness reduces pulsatility
- Reduced AQP4 polarization increases resistance
- Network architecture may degrade
- Waste accumulation (Aβ) further impairs flow

4.9 Bio-Inspired Engineering

4.9.1 Constructal Heat Exchangers

Biological principles inspire engineering design:

- Tree-shaped cooling networks for electronics
- Murray's Law for microfluidic distributors
- Hierarchical porous media for catalysis

4.9.2 Organ-on-Chip Vascularization

Applying constructal principles to in vitro systems:

- Design branching channel networks
- Optimize for uniform perfusion
- Balance shear stress across tissue

4.10 Summary

Key Concepts

- The **Constructal Law** states that flow systems evolve toward easier access
- **Murray's Law** ($r_0^3 = r_1^3 + r_2^3$) minimizes vascular pumping + metabolic cost
- **Allometric scaling** ($B \propto M^{3/4}$) emerges from network optimization
- **Entropy production minimization** provides a variational principle
- Disease often involves **deviation from optimal** network architecture

4.11 Further Reading

1. Bejan, A. (2016). *The Physics of Life*. St. Martin's Press.
2. West, G.B. et al. (1997). "A general model for the origin of allometric scaling laws in biology." *Science*.
3. Murray, C.D. (1926). "The physiological principle of minimum work." *PNAS*.

Part II

Biological Transport Systems

Chapter 5

Fluid Mechanics in Biology

5.1 The Navier-Stokes Equations

All biological fluid mechanics begins with the fundamental conservation laws. For an incompressible Newtonian fluid:

5.1.1 Conservation of Mass

$$\boldsymbol{\nabla} \cdot \mathbf{u} = 0 \tag{5.1}$$

5.1.2 Conservation of Momentum

$$\rho \left(\frac{\partial \mathbf{u}}{\partial t} + \mathbf{u} \cdot \boldsymbol{\nabla} \mathbf{u} \right) = -\boldsymbol{\nabla} p + \mu \nabla^2 \mathbf{u} + \mathbf{f} \tag{5.2}$$

where:

- $\mathbf{u}$ = velocity field [m/s]
- p = pressure [Pa]
- ρ = density [kg/m^3]
- μ = dynamic viscosity [Pa·s]
- $\mathbf{f}$ = body forces per unit volume [N/m^3]

5.2 Low Reynolds Number: Stokes Flow

5.2.1 The Mesoscale Regime

At the mesoscale, flow is dominated by viscous forces. The Reynolds number:

$$\mathrm{Re} = \frac{\rho U L}{\mu} = \frac{U L}{\nu} \tag{5.3}$$

For biological flows at the mesoscale:

System	Velocity	Length	Re
Perivascular space (PVS)	10–100 μm/s	20–100 μm	10^{-3}–10^{-2}
Capillary blood flow	0.5–1 mm/s	5–10 μm	10^{-3}–10^{-2}
CSF in ventricles	1–10 mm/s	1–10 mm	10^{-1}–10^{1}
Arteriole flow	10–100 mm/s	50–300 μm	10^{0}–10^{1}
Large artery	0.1–1 m/s	10–25 mm	10^{2}–10^{3}

5.2.2 Stokes Equations

When $\mathrm{Re} \ll 1$, the inertial terms can be neglected:

$$\boxed{0 = -\boldsymbol{\nabla} p + \mu \nabla^2 \mathbf{u} + \mathbf{f}} \tag{5.4}$$

Key properties of Stokes flow:

1. **Linearity**: Superposition of solutions is valid
2. **Reversibility**: Flow reverses exactly if forcing reverses
3. **Instantaneity**: Flow responds immediately to boundary changes
4. **No convective mixing**: Only diffusive transport at very low Re

5.2.3 Poiseuille Flow

Flow in a circular tube of radius R driven by pressure gradient $\Delta P/L$:

$$u(r) = \frac{\Delta P}{4\mu L}(R^2 - r^2) \tag{5.5}$$

Volume flow rate:

$$Q = \frac{\pi R^4 \Delta P}{8\mu L} \tag{5.6}$$

This is the foundation of Murray's Law—note the strong R^4 dependence.

5.3 Pulsatile Flow

5.3.1 The Womersley Number

For time-periodic flow with angular frequency ω:

$$\mathrm{Wo} = R\sqrt{\frac{\omega}{\nu}} \tag{5.7}$$

Physical interpretation:

- $\mathrm{Wo} \ll 1$: Quasi-steady flow (Poiseuille profile at each instant)
- $\mathrm{Wo} \sim 1$: Phase lag between pressure and velocity
- $\mathrm{Wo} \gg 1$: Flat velocity profile with thin oscillating boundary layer

Vessel/System	**Frequency**	**Wo**
PVS (cardiac)	1 Hz	0.1–0.5
Capillary (cardiac)	1 Hz	0.01–0.1
Arteriole (cardiac)	1 Hz	0.5–2
PVS (respiration)	0.2 Hz	0.05–0.2
Aorta (cardiac)	1 Hz	10–15

5.3.2 Womersley Solution

For sinusoidal pressure gradient in a tube:

$$u(r,t) = \text{Re}\left[\frac{1}{i\omega\rho}\frac{dP}{dx}\left(1 - \frac{J_0(\alpha r/R)}{J_0(\alpha)}\right)e^{i\omega t}\right] \tag{5.8}$$

where $\alpha = R\sqrt{i\omega/\nu}$ is the complex Womersley parameter and J_0 is the Bessel function of the first kind.

5.4 Non-Newtonian Biological Fluids

5.4.1 Shear-Thinning Behavior

Most biological fluids exhibit non-Newtonian behavior. Blood, mucus, and synovial fluid all show shear-thinning:

$$\mu(\dot{\gamma}) < \mu_0 \quad \text{as} \quad \dot{\gamma} \to \infty \tag{5.9}$$

where $\dot{\gamma}$ is the shear rate.

5.4.2 The Carreau-Yasuda Model

For blood rheology:

$$\mu(\dot{\gamma}) = \mu_\infty + (\mu_0 - \mu_\infty)\left[1 + (\lambda\dot{\gamma})^a\right]^{(n-1)/a} \tag{5.10}$$

Typical parameters for blood:

Parameter	Value	Meaning
μ_0	0.056 Pa·s	Zero-shear viscosity
μ_∞	0.00345 Pa·s	Infinite-shear viscosity
λ	3.313 s	Relaxation time
n	0.3568	Power-law exponent
a	2	Transition parameter

5.4.3 Power-Law Model

A simpler model for shear-thinning:

$$\mu = K\dot{\gamma}^{n-1} \tag{5.11}$$

where K is the consistency coefficient and $n < 1$ for shear-thinning fluids.

5.4.4 Herschel-Bulkley Model

For fluids with a yield stress (like mucus or blood at low shear):

$$\tau = \tau_y + K\dot{\gamma}^n \quad \text{if} \quad \tau > \tau_y \tag{5.12}$$

The fluid behaves as a solid below the yield stress τ_y.

5.5 Viscoelastic Fluids

5.5.1 The Oldroyd-B Model

Biological fluids often exhibit both viscous and elastic behavior:

$$\boldsymbol{\tau} + \lambda_1 \overset{\nabla}{\boldsymbol{\tau}} = \mu(\boldsymbol{D} + \lambda_2 \overset{\nabla}{\boldsymbol{D}}) \tag{5.13}$$

where $\overset{\nabla}{\boldsymbol{\tau}}$ denotes the upper-convected derivative:

$$\overset{\nabla}{\boldsymbol{\tau}} = \frac{D\boldsymbol{\tau}}{Dt} - (\boldsymbol{\nabla}\mathbf{u})^T \cdot \boldsymbol{\tau} - \boldsymbol{\tau} \cdot \boldsymbol{\nabla}\mathbf{u} \tag{5.14}$$

5.5.2 Maxwell Model

A simpler viscoelastic model:

$$\boldsymbol{\tau} + \lambda \frac{D\boldsymbol{\tau}}{Dt} = \mu \boldsymbol{D} \tag{5.15}$$

The relaxation time λ characterizes how quickly stress relaxes:

Fluid	λ
Blood	0.01–0.1 s
Mucus	0.1–10 s
Synovial fluid	0.1–1 s
Cerebrospinal fluid	Newtonian ($\lambda \approx 0$)

5.6 The Deborah Number

The ratio of relaxation time to observation time:

$$\mathrm{De} = \frac{\lambda}{t_{\text{obs}}} = \frac{\lambda U}{L} \tag{5.16}$$

- $\mathrm{De} \ll 1$: Fluid behavior dominates
- $\mathrm{De} \gg 1$: Solid-like behavior

5.7 Flow in Porous Media

5.7.1 Darcy's Law

For flow through porous tissue (extracellular matrix, brain parenchyma):

$$\mathbf{u} = -\frac{K}{\mu}\boldsymbol{\nabla} p \tag{5.17}$$

where K is the permeability [m^2].

5.7.2 Brinkman Equation

When both porous resistance and viscous effects matter:

$$0 = -\boldsymbol{\nabla} p + \mu_{\text{eff}} \nabla^2 \mathbf{u} - \frac{\mu}{K}\mathbf{u} \tag{5.18}$$

This is crucial for flow in perivascular spaces adjacent to brain tissue.

5.7.3 Permeability Values

Tissue	Permeability K	Reference
Brain parenchyma	10^{-17}–10^{-15} m^2	Jin et al. (2016)
Cartilage	10^{-16}–10^{-14} m^2	Mow et al. (1984)
Tumor tissue	10^{-15}–10^{-13} m^2	Jain (1987)
Muscle	10^{-14}–10^{-12} m^2	Various

5.8 Two-Phase and Multiphase Flows

5.8.1 The Fåhræus Effect

In small vessels (diameter < 300 μm), blood exhibits:

- **Cell-free layer**: RBCs migrate away from walls
- **Reduced hematocrit**: Tube hematocrit $<$ discharge hematocrit
- **Apparent viscosity**: Lower than expected from bulk properties

5.8.2 Fåhræus-Lindqvist Effect

Apparent viscosity decreases with tube diameter below 300 μm:

$$\mu_{\text{app}} = \mu_{\text{plasma}} \left[1 + (4.0 - 1) \frac{(1 - H_D)^C - 1}{(1 - 0.45)^C - 1} \right] \tag{5.19}$$

where H_D is the discharge hematocrit and C depends on diameter.

5.9 Computational Approaches

5.9.1 Finite Element Methods

Traditional approach for complex geometries:

- Weak formulation of Navier-Stokes
- Inf-sup stable element pairs (Taylor-Hood, MINI)
- Stabilization for high Re (SUPG, PSPG)

5.9.2 Lattice Boltzmann Methods

Particularly well-suited for mesoscale biology:

- Natural handling of complex boundaries
- Easy parallelization on GPUs
- Extension to non-Newtonian and multiphase flows
- See Chapter 9 for detailed treatment

5.9.3 Immersed Boundary Methods

For fluid-structure interaction:

- Eulerian fluid, Lagrangian structure
- Regularized delta function for force spreading
- See Chapter 7 for detailed treatment

5.10 Biological Fluid Properties

Fluid	**Density** [kg/m^3]	**Viscosity** [mPa·s]	**Notes**
Water	1000	1.0	Reference
Blood (whole)	1060	3–4	Shear-thinning
Plasma	1025	1.2	Newtonian
CSF	1007	0.7–1.0	Newtonian
Mucus	1000–1050	10–1000	Viscoelastic
Synovial fluid	1010	10–10000	Highly variable

5.11 Summary

Key Concepts

- **Low Reynolds number**: Mesoscale flows are viscous-dominated, described by Stokes equations
- **Womersley number**: Determines importance of pulsatility; Wo $<$ 1 at most mesoscale systems
- **Non-Newtonian effects**: Blood is shear-thinning (Carreau-Yasuda); mucus is viscoelastic
- **Porous media**: Darcy/Brinkman equations for flow through tissue
- **Poiseuille law**: $Q \propto R^4$ explains sensitivity of flow to vessel radius

5.12 Further Reading

1. Fung, Y.C. (1993). *Biomechanics: Mechanical Properties of Living Tissues.* Springer.
2. Pedley, T.J. (1980). *The Fluid Mechanics of Large Blood Vessels.* Cambridge.
3. Happel, J. & Brenner, H. (1983). *Low Reynolds Number Hydrodynamics.* Kluwer.
4. Ethier, C.R. & Simmons, C.A. (2007). *Introductory Biomechanics.* Cambridge.

Chapter 6

Mass Transport and Reaction

6.1 The Advection-Diffusion-Reaction Equation

Mass transport in biological systems is governed by the conservation equation:

$$\boxed{\frac{\partial C}{\partial t} + \mathbf{u} \cdot \boldsymbol{\nabla} C = D \nabla^2 C + R(C)} \tag{6.1}$$

where:

- C = concentration [mol/m^3] or [kg/m^3]
- $\mathbf{u}$ = velocity field [m/s]
- D = diffusion coefficient [m^2/s]
- $R(C)$ = reaction/source term [mol/(m^3·s)]

6.2 The Peclet Number

The ratio of advective to diffusive transport:

$$\mathrm{Pe} = \frac{UL}{D} \tag{6.2}$$

6.2.1 Typical Values in Biology

System	**Solute**	**D [m^2/s]**	**Pe**
PVS CSF flow	Small molecules	10^{-9}	1–100
PVS CSF flow	Aβ (4 kDa)	10^{-10}	10–1000
Capillary O_2	Oxygen	2×10^{-9}	100–1000
Intestinal lumen	Glucose	6×10^{-10}	1000–10000
Synaptic cleft	Neurotransmitter	5×10^{-10}	<1

6.2.2 Transport Regimes

- Pe $\ll 1$: **Diffusion-dominated** — concentration spreads uniformly
- Pe ~ 1: **Mixed regime** — both mechanisms important
- Pe $\gg 1$: **Advection-dominated** — solute carried by flow; thin boundary layers

6.3 Diffusion in Biological Systems

6.3.1 Fick's Laws

First law (flux):

$$\mathbf{J} = -D\boldsymbol{\nabla} C \tag{6.3}$$

Second law (evolution):

$$\frac{\partial C}{\partial t} = D\nabla^2 C \tag{6.4}$$

6.3.2 Diffusion Coefficients

The Stokes-Einstein relation for spherical molecules:

$$D = \frac{k_B T}{6\pi\mu r_H} \tag{6.5}$$

where r_H is the hydrodynamic radius.

Solute	**MW [Da]**	r_H **[nm]**	D **[m^2/s]**
O_2	32	0.2	2×10^{-9}
Glucose	180	0.4	6×10^{-10}
Aβ_{1-40}	4300	1.5	1.5×10^{-10}
Albumin	66000	3.5	6×10^{-11}
IgG	150000	5.3	4×10^{-11}

6.3.3 Effective Diffusion in Porous Media

In tissue, diffusion is hindered by the extracellular matrix:

$$D_{\text{eff}} = \frac{D_0 \varepsilon}{\tau} \tag{6.6}$$

where:

- ε = porosity (volume fraction)
- τ = tortuosity factor (>1)

For brain tissue: $\varepsilon \approx 0.2$, $\tau \approx 1.6$, giving $D_{\text{eff}} \approx 0.4 D_0$.

6.4 The Damköhler Number

The ratio of reaction rate to transport rate:

$$\text{Da} = \frac{\tau_{\text{transport}}}{\tau_{\text{reaction}}} = \frac{L^2/D}{1/k} = \frac{kL^2}{D} \tag{6.7}$$

For advection-dominated systems:

$$\text{Da} = \frac{kL}{U} \tag{6.8}$$

6.4.1 Reaction-Transport Regimes

- Da $\ll 1$: **Transport-limited** — reaction is fast, transport controls
- Da ~ 1: **Mixed regime** — both rates comparable
- Da $\gg 1$: **Reaction-limited** — transport is fast, kinetics controls

6.5 Enzyme Kinetics

6.5.1 Michaelis-Menten Kinetics

For enzyme-catalyzed reactions:

$$R = \frac{V_{\max} C}{K_m + C} \tag{6.9}$$

where:

- $V_{\max}$ = maximum reaction rate
- K_m = Michaelis constant (concentration at half-max rate)

6.5.2 Limiting Cases

First-order kinetics ($C \ll K_m$):

$$R \approx \frac{V_{\max}}{K_m} C = k_1 C \tag{6.10}$$

Zero-order kinetics ($C \gg K_m$):

$$R \approx V_{\max} \tag{6.11}$$

6.5.3 Hill Equation

For cooperative binding (e.g., oxygen to hemoglobin):

$$\theta = \frac{C^n}{K_d^n + C^n} \tag{6.12}$$

where n is the Hill coefficient:

- $n = 1$: No cooperativity
- $n > 1$: Positive cooperativity (hemoglobin: $n \approx 2.8$)
- $n < 1$: Negative cooperativity

6.6 Oxygen Transport

6.6.1 The Oxygen Dissociation Curve

Hemoglobin saturation follows the Hill equation:

$$S_{O_2} = \frac{P_{O_2}^n}{P_{50}^n + P_{O_2}^n} \tag{6.13}$$

where $P_{50} \approx 26$ mmHg (oxygen partial pressure at 50% saturation).

6.6.2 Krogh Cylinder Model

Classic model for oxygen delivery from capillary to tissue:

$$\frac{1}{r}\frac{d}{dr}\left(r\frac{dP_{O_2}}{dr}\right) = \frac{M_0}{\alpha D_{O_2}} \tag{6.14}$$

where:

- M_0 = metabolic consumption rate [mol O_2/(m^3·s)]
- α = solubility coefficient
- D_{O_2} = diffusion coefficient

6.6.3 Critical Tissue Radius

The maximum radius tissue can be supplied from a single capillary:

$$R_t = \sqrt{\frac{4\alpha D_{O_2}(P_c - P_{\min})}{M_0}} \tag{6.15}$$

Typical value: $R_t \approx 100$–200 μm, explaining capillary spacing.

6.7 Mass Transfer Coefficients

6.7.1 Boundary Layer Theory

At high Peclet number, concentration gradients are confined to thin boundary layers. The mass transfer coefficient:

$$k_m = \frac{D}{\delta} \tag{6.16}$$

where δ is the boundary layer thickness.

6.7.2 Sherwood Number

Dimensionless mass transfer coefficient:

$$\text{Sh} = \frac{k_m L}{D} \tag{6.17}$$

Correlations depend on geometry and flow regime:

- Flat plate, laminar: $\text{Sh} = 0.664\text{Re}^{1/2}\text{Sc}^{1/3}$
- Pipe, laminar: $\text{Sh} = 1.86(\text{Re} \cdot \text{Sc} \cdot d/L)^{1/3}$
- Sphere: $\text{Sh} = 2 + 0.6\text{Re}^{1/2}\text{Sc}^{1/3}$

where $\text{Sc} = \nu/D$ is the Schmidt number.

6.8 Clearance Mechanisms

6.8.1 Glymphatic Clearance

Waste removal from brain involves:

1. CSF entry via peri-arterial spaces
2. Convective transport through parenchyma (controversial)
3. Exit via peri-venous spaces
4. Drainage to lymphatics

The clearance rate can be modeled as:

$$\frac{dC}{dt} = -k_{\text{clear}} C + S \tag{6.18}$$

where k_{clear} is the clearance rate constant and S is production.

6.8.2 Renal Clearance

Glomerular filtration rate (GFR):

$$\text{GFR} = K_f \cdot [(P_{GC} - P_{BS}) - (\pi_{GC} - \pi_{BS})] \tag{6.19}$$

where:

- K_f = filtration coefficient
- P = hydrostatic pressures
- π = oncotic pressures
- GC = glomerular capillary, BS = Bowman's space

6.8.3 Hepatic Clearance

The "well-stirred" model:

$$\text{CL}_H = \frac{Q_H \cdot f_u \cdot \text{CL}_{\text{int}}}{Q_H + f_u \cdot \text{CL}_{\text{int}}} \tag{6.20}$$

where Q_H is hepatic blood flow, f_u is unbound fraction, and CL_{int} is intrinsic clearance.

6.9 Coupled Transport-Reaction Systems

6.9.1 Thiele Modulus

For diffusion with first-order reaction inside a porous medium:

$$\phi = L\sqrt{\frac{k}{D}} \tag{6.21}$$

6.9.2 Effectiveness Factor

The ratio of actual to ideal reaction rate:

$$\eta = \frac{\tanh \phi}{\phi} \quad \text{(slab geometry)} \tag{6.22}$$

- $\phi \ll 1$: $\eta \approx 1$ (reaction-limited, uniform concentration)
- $\phi \gg 1$: $\eta \approx 1/\phi$ (diffusion-limited, steep gradients)

6.10 Multi-Species Transport

6.10.1 Coupled Reaction-Diffusion

For n interacting species:

$$\frac{\partial C_i}{\partial t} = D_i \nabla^2 C_i + R_i(C_1, C_2, \ldots, C_n) \tag{6.23}$$

Examples in biology:

- Calcium waves: Ca^{2+} release triggers further release
- Morphogen gradients: Production, degradation, and transport
- Neurotransmitter dynamics: Release, diffusion, uptake, degradation

6.10.2 Turing Patterns

When diffusion coefficients differ significantly, reaction-diffusion systems can generate spatial patterns:

$$\frac{\partial u}{\partial t} = D_u \nabla^2 u + f(u, v) \tag{6.24}$$

$$\frac{\partial v}{\partial t} = D_v \nabla^2 v + g(u, v) \tag{6.25}$$

Instability requires:

- $D_v \gg D_u$ (inhibitor diffuses faster than activator)
- Specific kinetics ($f_u > 0$, $g_v < 0$, $f_u g_v - f_v g_u > 0$)

6.11 Numerical Methods

6.11.1 Finite Difference

Central difference for diffusion:

$$\nabla^2 C \approx \frac{C_{i+1} - 2C_i + C_{i-1}}{\Delta x^2} \tag{6.26}$$

Upwind scheme for advection (high Pe):

$$u \frac{\partial C}{\partial x} \approx u \frac{C_i - C_{i-1}}{\Delta x} \quad (u > 0) \tag{6.27}$$

6.11.2 Stability Criteria

For explicit time integration:

$$\Delta t < \frac{\Delta x^2}{2D} \quad \text{(diffusion)} \tag{6.28}$$

$$\Delta t < \frac{\Delta x}{|u|} \quad \text{(advection, CFL condition)} \tag{6.29}$$

6.11.3 Lattice Boltzmann for Advection-Diffusion

Separate distribution function for concentration:

$$g_i(\mathbf{x} + \mathbf{c}_i \Delta t, t + \Delta t) - g_i(\mathbf{x}, t) = -\frac{1}{\tau_g}(g_i - g_i^{eq}) \tag{6.30}$$

with $D = c_s^2(\tau_g - 0.5)\Delta t$.

6.12 Applications to Mesoscale Biology

6.12.1 Intestinal Absorption

The unstirred water layer (UWL) at the villus surface:

- Thickness: 100–400 μm
- Creates diffusion barrier for nutrients
- Stirring by villi movements reduces effective UWL

Effective permeability:

$$P_{\text{eff}} = \frac{1}{1/P_{\text{UWL}} + 1/P_{\text{membrane}}} \tag{6.31}$$

6.12.2 Drug Delivery

Tissue penetration limited by:

- Vascular permeability (extravasation)
- Interstitial transport (diffusion + convection)
- Cellular uptake and metabolism

The Krogh-length concept generalizes: drugs penetrate $\sim \sqrt{D/k}$ from vessel.

6.13 Summary

Key Concepts

- The **Peclet number** (Pe $= UL/D$) determines whether advection or diffusion dominates
- The **Damköhler number** (Da) compares reaction and transport time scales
- **Michaelis-Menten kinetics** describes enzyme-catalyzed reactions
- **Oxygen delivery** follows Krogh cylinder model with critical tissue radius
- **Clearance** mechanisms (glymphatic, renal, hepatic) remove waste products
- **Boundary layers** at high Pe confine concentration gradients to thin regions

6.14 Further Reading

1. Bird, R.B., Stewart, W.E., Lightfoot, E.N. (2007). *Transport Phenomena.* Wiley.
2. Deen, W.M. (2012). *Analysis of Transport Phenomena.* Oxford.
3. Truskey, G.A., Yuan, F., Katz, D.F. (2009). *Transport Phenomena in Biological Systems.* Pearson.
4. Fournier, R.L. (2011). *Basic Transport Phenomena in Biomedical Engineering.* CRC Press.

Chapter 7

Tissue Mechanics and Fluid-Structure Interaction

7.1 Introduction to Tissue Mechanics

Biological tissues exhibit complex mechanical behavior that differs fundamentally from engineering materials:

- Large deformations (strains of 10–100%)
- Nonlinear stress-strain relationships
- Anisotropy (direction-dependent properties)
- Viscoelasticity (time-dependent response)
- Active contraction (muscle, smooth muscle)
- Growth and remodeling

7.2 Continuum Mechanics Framework

7.2.1 Kinematics of Deformation

The deformation gradient tensor maps material points from reference ($\mathbf{X}$) to current ($\mathbf{x}$) configuration:

$$\boldsymbol{F} = \frac{\partial \mathbf{x}}{\partial \mathbf{X}} \tag{7.1}$$

The Jacobian (volume ratio):

$$J = \det(\boldsymbol{F}) \tag{7.2}$$

For incompressible materials: $J = 1$.

7.2.2 Strain Measures

Right Cauchy-Green tensor:

$$\boldsymbol{C} = \boldsymbol{F}^T \boldsymbol{F} \tag{7.3}$$

Green-Lagrange strain:

$$\boldsymbol{E} = \frac{1}{2}(\boldsymbol{C} - \boldsymbol{I}) \tag{7.4}$$

Principal stretches λ_i are eigenvalues of $\boldsymbol{F}$.

7.2.3 Stress Measures

Cauchy stress (true stress in current configuration):

$$\boldsymbol{\sigma} = \frac{1}{J}\boldsymbol{P}\boldsymbol{F}^T \tag{7.5}$$

First Piola-Kirchhoff stress (force per reference area):

$$\boldsymbol{P} = J\boldsymbol{\sigma}\boldsymbol{F}^{-T} \tag{7.6}$$

Second Piola-Kirchhoff stress (work conjugate to $\boldsymbol{E}$):

$$\boldsymbol{S} = \boldsymbol{F}^{-1}\boldsymbol{P} \tag{7.7}$$

7.3 Hyperelastic Constitutive Models

Hyperelastic materials derive stress from a strain energy density function W:

$$\boldsymbol{S} = 2\frac{\partial W}{\partial \boldsymbol{C}} \tag{7.8}$$

7.3.1 Neo-Hookean Model

The simplest hyperelastic model:

$$W = \frac{\mu}{2}(I_1 - 3) \tag{7.9}$$

where $I_1 = \text{tr}(\boldsymbol{C}) = \lambda_1^2 + \lambda_2^2 + \lambda_3^2$.
For nearly incompressible materials, add penalty:

$$W = \frac{\mu}{2}(I_1 - 3) + \frac{\kappa}{2}(J-1)^2 \tag{7.10}$$

7.3.2 Mooney-Rivlin Model

Adds second invariant dependence:

$$W = C_1(I_1 - 3) + C_2(I_2 - 3) \tag{7.11}$$

where $I_2 = \frac{1}{2}[(\text{tr}\boldsymbol{C})^2 - \text{tr}(\boldsymbol{C}^2)]$.

7.3.3 Ogden Model

More general strain energy:

$$W = \sum_{p=1}^{N} \frac{\mu_p}{\alpha_p}(\lambda_1^{\alpha_p} + \lambda_2^{\alpha_p} + \lambda_3^{\alpha_p} - 3) \tag{7.12}$$

Commonly $N = 3$ with six fitted parameters.

7.3.4 Fung Exponential Model

For soft tissues exhibiting strain-stiffening:

$$W = \frac{c}{2}(e^Q - 1) \tag{7.13}$$

where Q is a quadratic function of strain components, e.g.:

$$Q = b_1 E_{11}^2 + b_2 E_{22}^2 + 2b_3 E_{11}E_{22} + b_4 E_{12}^2 \tag{7.14}$$

7.4 Typical Tissue Properties

Tissue	Young's Modulus	Behavior	Model
Brain	0.1–1 kPa	Soft, viscoelastic	Neo-Hookean
Liver	1–10 kPa	Soft, viscoelastic	Ogden
Artery wall	0.1–1 MPa	Anisotropic, stiffening	Fung, HGO
Cartilage	1–10 MPa	Poroelastic	Biphasic
Tendon	0.1–1 GPa	Anisotropic, stiff	Fiber-reinforced
Bone	10–20 GPa	Hard, brittle	Linear elastic

7.5 Anisotropic Models

7.5.1 Fiber-Reinforced Materials

For tissues with preferred fiber directions (arteries, heart, tendons):

$$W = W_{\text{matrix}}(I_1, I_2) + W_{\text{fiber}}(I_4, I_6) \tag{7.15}$$

where $I_4 = \mathbf{a}_0 \cdot \boldsymbol{C} \cdot \mathbf{a}_0$ is the square of fiber stretch.

7.5.2 Holzapfel-Gasser-Ogden (HGO) Model

For arterial tissue:

$$W = \frac{\mu}{2}(I_1 - 3) + \frac{k_1}{2k_2} \sum_{i=4,6} \left(e^{k_2 (I_i - 1)^2} - 1 \right) \tag{7.16}$$

This captures the J-shaped stress-strain curve of arteries.

7.6 Viscoelasticity

7.6.1 Quasi-Linear Viscoelasticity (QLV)

Fung's approach separates elastic response from time-dependent relaxation:

$$\sigma(t) = \int_{-\infty}^{t} G(t - \tau) \frac{\partial \sigma^e}{\partial \tau} d\tau \tag{7.17}$$

where $G(t)$ is the reduced relaxation function and σ^e is the elastic stress.

7.6.2 Prony Series

The relaxation function is often represented as:

$$G(t) = G_\infty + \sum_{i=1}^{N} G_i e^{-t/\tau_i} \tag{7.18}$$

with relaxation times τ_i spanning multiple decades.

7.6.3 Standard Linear Solid

Simple three-parameter model:

$$\sigma + \tau_\sigma \frac{d\sigma}{dt} = E_R \left(\varepsilon + \tau_\varepsilon \frac{d\varepsilon}{dt} \right) \tag{7.19}$$

7.7 Fluid-Structure Interaction

7.7.1 The FSI Problem

Coupling between fluid and deformable solid requires:

- **Kinematic coupling**: Velocity continuity at interface
- **Dynamic coupling**: Force equilibrium at interface
- **Geometric coupling**: Interface position updates

7.7.2 Coupling Conditions

At the fluid-structure interface Γ:

$$\mathbf{u}_f = \frac{\partial \mathbf{d}_s}{\partial t} \qquad \text{(no-slip)} \tag{7.20}$$

$$\boldsymbol{\sigma}_f \cdot \mathbf{n} = \boldsymbol{\sigma}_s \cdot \mathbf{n} \qquad \text{(traction continuity)} \tag{7.21}$$

7.7.3 Monolithic vs. Partitioned Approaches

Monolithic: Solve fluid and solid simultaneously

- Pros: Robust, handles strong coupling
- Cons: Complex implementation, large systems

Partitioned: Separate solvers with interface coupling

- Pros: Reuse existing codes, modular
- Cons: May require sub-iterations, added mass instability

7.8 The Immersed Boundary Method

7.8.1 Peskin's Formulation

The Immersed Boundary Method (IBM) represents elastic structures on a Lagrangian mesh while solving fluid on a fixed Eulerian grid.

Fluid equations (Eulerian):

$$\rho\left(\frac{\partial \mathbf{u}}{\partial t} + \mathbf{u} \cdot \boldsymbol{\nabla}\mathbf{u}\right) = -\boldsymbol{\nabla} p + \mu \nabla^2 \mathbf{u} + \mathbf{f} \tag{7.22}$$

$$\boldsymbol{\nabla} \cdot \mathbf{u} = 0 \tag{7.23}$$

Force spreading (Lagrangian to Eulerian):

$$\mathbf{f}(\mathbf{x}, t) = \int_\Gamma \mathbf{F}(s, t)\delta(\mathbf{x} - \mathbf{X}(s, t))\, ds \tag{7.24}$$

Velocity interpolation (Eulerian to Lagrangian):

$$\frac{\partial \mathbf{X}}{\partial t}(s, t) = \mathbf{u}(\mathbf{X}(s, t), t) = \int \mathbf{u}(\mathbf{x}, t)\delta(\mathbf{x} - \mathbf{X}(s, t))\, d\mathbf{x} \tag{7.25}$$

7.8.2 Regularized Delta Functions

The Dirac delta is regularized for numerical implementation:

$$\delta_h(\mathbf{x}) = \frac{1}{h^d}\phi\left(\frac{x}{h}\right)\phi\left(\frac{y}{h}\right)\phi\left(\frac{z}{h}\right) \tag{7.26}$$

Common choices for ϕ:

- 2-point: $\phi(r) = \frac{1}{2}(1 + \cos(\pi r))$ for $|r| < 1$
- 4-point Peskin: Smoother, better volume conservation
- 6-point Roma: Even smoother but wider support

7.8.3 Elastic Force Calculation

For a simple elastic fiber:

$$\mathbf{F}(s,t) = \frac{\partial}{\partial s}\left(T(s,t)\frac{\partial \mathbf{X}}{\partial s}\right) \tag{7.27}$$

where the tension T depends on fiber stretch.

7.9 IBM in Lattice Boltzmann Framework

7.9.1 Algorithm

1. Stream and collide LBM distribution functions
2. Compute fluid velocity from distributions
3. Interpolate velocity to Lagrangian points
4. Compute elastic forces on boundary
5. Spread forces to Eulerian grid
6. Update Lagrangian point positions

7.9.2 Force Spreading with LBM

The momentum exchange is:

$$\Delta\mathbf{G}(\mathbf{x}) = \sum_k \mathbf{F}_k\,\phi_h(\mathbf{x} - \mathbf{X}_k)\Delta s \tag{7.28}$$

This is added to the body force in the LBM collision step.

7.10 Applications at the Mesoscale

7.10.1 Arterial Pulsation

The artery wall deforms cyclically with blood pressure:

- Pressure variation: 80–120 mmHg (systemic)
- Wall strain: 5–10%
- Womersley number: Wo $\sim$ 3–5

This deformation drives perivascular space flow.

7.10.2 Intestinal Villi Motion

Villi undergo rhythmic contractions:

- Frequency: 10–15 contractions/minute
- Shortening: 10–30% of length
- Enhances nutrient mixing in unstirred layer

7.10.3 Alveolar Breathing Mechanics

Lung inflation involves:

- Surface tension (surfactant-modified)
- Tissue elasticity
- Airway FSI
- Regional ventilation heterogeneity

7.11 Poroelasticity

7.11.1 Biot's Theory

For fluid-saturated porous media (cartilage, brain tissue):

$$\boldsymbol{\nabla} \cdot \boldsymbol{\sigma}' + \alpha \boldsymbol{\nabla} p = \mathbf{0} \tag{7.29}$$

$$\alpha \frac{\partial \varepsilon_v}{\partial t} + \frac{1}{M} \frac{\partial p}{\partial t} + \boldsymbol{\nabla} \cdot \mathbf{q} = 0 \tag{7.30}$$

where:

- $\boldsymbol{\sigma}'$ = effective stress in solid skeleton
- α = Biot coefficient
- M = Biot modulus
- $\mathbf{q}$ = Darcy flux

7.11.2 Consolidation Time Scale

The characteristic time for pore pressure diffusion:

$$t_c = \frac{L^2}{c_v} \tag{7.31}$$

where $c_v = KM/(\alpha^2 M + \mu_s/\lambda_s)$ is the consolidation coefficient.

7.12 Active Tissue Mechanics

7.12.1 Smooth Muscle Contraction

Smooth muscle in vessel walls generates active stress:

$$\sigma_{\text{total}} = \sigma_{\text{passive}}(\lambda) + \sigma_{\text{active}}(\lambda, [\text{Ca}^{2+}], t) \tag{7.32}$$

Vasomotion creates traveling waves of contraction.

7.12.2 Hill's Muscle Model

For skeletal/cardiac muscle:

$$(F + a)(v + b) = (F_0 + a)b \tag{7.33}$$

where F is force, v is shortening velocity, F_0 is isometric force, and a, b are parameters.

7.13 Numerical Considerations

7.13.1 Time Step Restrictions

FSI stability requires:

$$\Delta t < \min\left(\frac{\Delta x}{c}, \frac{\rho_s h^2}{\mu}, \frac{\Delta x}{U}\right) \tag{7.34}$$

where c is the elastic wave speed.

7.13.2 Added Mass Effect

When $\rho_s \approx \rho_f$, strong coupling is essential to avoid instability. Sub-iterations or monolithic schemes may be needed.

7.13.3 Volume Conservation

IBM can suffer from volume leakage. Remedies:

- Feedback forcing to maintain volume
- Direct forcing schemes
- Multi-direct forcing iterations

7.14 Summary

Key Concepts

- **Hyperelastic models** (Neo-Hookean, Mooney-Rivlin, Fung) describe nonlinear tissue mechanics
- **Viscoelasticity** captures time-dependent response via relaxation functions
- **FSI** couples fluid and solid through interface conditions
- **Immersed Boundary Method** handles moving boundaries on fixed fluid grids
- **Poroelasticity** describes fluid-saturated deformable tissues
- **Active mechanics** includes muscle contraction and vasomotion

7.15 Further Reading

1. Holzapfel, G.A. (2000). *Nonlinear Solid Mechanics*. Wiley.
2. Humphrey, J.D. (2002). *Cardiovascular Solid Mechanics*. Springer.
3. Peskin, C.S. (2002). "The immersed boundary method." *Acta Numerica*.

4. Cowin, S.C. & Doty, S.B. (2007). *Tissue Mechanics.* Springer.

Chapter 8

Mechanotransduction

8.1 Introduction to Mechanotransduction

Mechanotransduction is the process by which cells convert mechanical stimuli into biochemical signals. This is fundamental to:

- Vascular function (endothelial shear sensing)
- Bone remodeling (Wolff's law)
- Hearing (hair cell deflection)
- Touch (skin mechanoreceptors)
- Proprioception (muscle spindles)
- Development and morphogenesis

8.2 Mechanical Stimuli in Biology

8.2.1 Types of Mechanical Forces

Force Type	**Example**	**Magnitude**
Shear stress	Blood flow on endothelium	1–70 dyne/cm^2
Hydrostatic pressure	Interstitial fluid	0–20 mmHg
Tensile strain	Lung expansion	5–20%
Compressive strain	Cartilage loading	10–50%
Substrate stiffness	ECM rigidity	0.1–100 kPa

8.2.2 Time Scales of Mechanical Stimuli

Stimulus	**Frequency**	**Cellular Response**
Cardiac pulsation	1–2 Hz	Rapid ion flux
Respiration	0.1–0.3 Hz	Moderate adaptation
Peristalsis	0.05–0.1 Hz	Slow adaptation
Static loading	Continuous	Remodeling (hours-days)

8.3 Mechanosensitive Ion Channels

8.3.1 Piezo Channels

Piezo1 and Piezo2 are the primary mechanosensitive ion channels in mammals:

Structure:

- Large trimeric proteins (∼300 kDa per subunit)
- Curved blade-like structure
- Mechanically gated pore

Gating mechanism:

$$P_{\text{open}} = \frac{1}{1 + \exp\left(-\frac{\sigma - \sigma_{1/2}}{\sigma_k}\right)} \tag{8.1}$$

where:

- σ = membrane tension
- $\sigma_{1/2}$ = half-activation tension (∼1–3 mN/m)
- σ_k = sensitivity parameter

8.3.2 Piezo1 Distribution

Tissue/Cell	Function
Endothelium	Shear stress sensing, vasodilation
Red blood cells	Volume regulation
Epithelial cells	Pressure sensing
Osteocytes	Bone mechanosensing
Bladder	Filling detection

8.3.3 Piezo2 Distribution

Tissue/Cell	Function
Sensory neurons (DRG)	Touch sensation
Merkel cells	Light touch
Proprioceptors	Body position
Airway epithelium	Respiration sensing

8.3.4 Other Mechanosensitive Channels

- **TRPV4**: Osmotic pressure, temperature
- **TREK/TRAAK**: Two-pore domain K^+ channels
- **MscL/MscS**: Bacterial mechanosensitive channels
- **ENaC**: Epithelial Na^+ channel (fluid shear)

8.4 Calcium Signaling in Mechanotransduction

8.4.1 Calcium as Second Messenger

Piezo channels are permeable to Ca^{2+}, triggering intracellular signaling:

$$\text{Mechanical force} \rightarrow \text{Piezo opening} \rightarrow Ca^{2+} \text{ influx} \rightarrow \text{Downstream signals} \tag{8.2}$$

8.4.2 Calcium Dynamics Model

Cytosolic calcium evolution:

$$\frac{d[Ca^{2+}]_c}{dt} = J_{\text{Piezo}} + J_{\text{ER}} - J_{\text{pump}} - J_{\text{buffer}} \tag{8.3}$$

where:

- J_{Piezo} = influx through mechanosensitive channels
- J_{ER} = release from endoplasmic reticulum
- J_{pump} = SERCA pump uptake
- J_{buffer} = binding to calcium buffers

8.4.3 Piezo-Mediated Calcium Influx

$$J_{\text{Piezo}} = g_{\text{Piezo}} \cdot P_{\text{open}}(\sigma) \cdot (V - E_{\text{Ca}}) \cdot N_{\text{Piezo}} \tag{8.4}$$

where:

- g_{Piezo} = single channel conductance (∼25–30 pS)
- V = membrane potential
- E_{Ca} = calcium reversal potential
- N_{Piezo} = number of channels

8.4.4 Calcium Wave Propagation

Calcium signals can propagate through tissue via:

$$\frac{\partial[Ca^{2+}]}{\partial t} = D_{\text{Ca}} \nabla^2 \left[Ca^{2+}\right] + J_{\text{IP}_3\text{R}}([Ca^{2+}], [IP_3]) \tag{8.5}$$

The IP_3 receptor exhibits calcium-induced calcium release (CICR), enabling wave propagation.

8.5 The YAP/TAZ Pathway

8.5.1 Overview

YAP (Yes-associated protein) and TAZ (transcriptional coactivator with PDZ-binding motif) are mechanosensitive transcription factors:

$$\text{Soft substrate} \rightarrow \text{YAP cytoplasmic} \rightarrow \text{Quiescence/Differentiation} \tag{8.6}$$

$$\text{Stiff substrate} \rightarrow \text{YAP nuclear} \rightarrow \text{Proliferation/Survival} \tag{8.7}$$

8.5.2 Regulation by Mechanics

Mechanical Cue	Effect	Mechanism
Stiff ECM	YAP nuclear	Actin tension, LATS inhibition
Cell spreading	YAP nuclear	Cytoskeletal tension
Low density	YAP nuclear	Reduced contact inhibition
Soft ECM	YAP cytoplasmic	LATS activation, phosphorylation
High density	YAP cytoplasmic	Hippo pathway activation

8.5.3 Hippo Pathway

The Hippo pathway phosphorylates and inactivates YAP/TAZ:

$$\text{MST1/2} \rightarrow \text{LATS1/2} \rightarrow \text{YAP-P} \rightarrow \text{14-3-3 binding} \rightarrow \text{Cytoplasmic retention} \tag{8.8}$$

Mechanical forces inhibit Hippo signaling, allowing YAP nuclear translocation.

8.5.4 Mathematical Model

YAP nuclear/cytoplasmic ratio:

$$\frac{d[\text{YAP}_n]}{dt} = k_{\text{in}}(\sigma) \cdot [\text{YAP}_c] - k_{\text{out}} \cdot [\text{YAP}_n] \tag{8.9}$$

where k_{in} depends on mechanical stress σ through cytoskeletal tension.

8.6 Shear Stress Sensing in Endothelium

8.6.1 Mechanosensors

Endothelial cells sense shear stress through:

- **Glycocalyx**: Surface layer deformation
- **Primary cilia**: Bending in flow
- **Piezo1**: Membrane tension from flow
- **PECAM-1/VE-cadherin/VEGFR2**: Junctional complex
- **Integrins**: Cytoskeletal force transmission

8.6.2 Physiological Shear Stress Ranges

Location	Shear Stress	Phenotype
Straight artery	15–70 dyne/cm^2	Atheroprotective
Bifurcation (low)	0–4 dyne/cm^2	Atheroprone
Bifurcation (oscillatory)	$\pm$4 dyne/cm^2	Atheroprone
Capillary	10–20 dyne/cm^2	Normal
Vein	1–6 dyne/cm^2	Normal venous

8.6.3 Nitric Oxide Response

Shear stress triggers endothelial nitric oxide synthase (eNOS) activation:

$$\tau \rightarrow \text{Ca}^{2+} \uparrow \rightarrow \text{eNOS activation} \rightarrow \text{NO production} \rightarrow \text{Vasodilation} \tag{8.10}$$

Time scales:

- Acute response: seconds (Ca^{2+}-dependent)
- Sustained response: hours (eNOS expression)

8.7 Focal Adhesions and Force Transmission

8.7.1 Structure

Focal adhesions connect ECM to cytoskeleton:

- **Integrins**: Transmembrane receptors binding ECM
- **Talin**: Links integrin to actin
- **Vinculin**: Reinforces talin-actin connection
- **FAK**: Focal adhesion kinase (signaling)
- **Paxillin**: Scaffolding protein

8.7.2 Force-Dependent Assembly

Focal adhesions grow under tension:

$$\frac{dA}{dt} = k_{\text{on}} \cdot f(\text{stress}) - k_{\text{off}} \cdot A \tag{8.11}$$

Above a threshold force, adhesions mature and signal.

8.7.3 Traction Force Microscopy

Cells exert forces on substrates, measurable by:

- Pillar deflection
- Gel deformation (with embedded beads)
- FRET-based tension sensors

Typical traction stresses: 1–10 kPa.

8.8 Computational Modeling of Mechanotransduction

8.8.1 Multi-Scale Framework

Scale	Model	Output
Tissue	Continuum (FEM)	Stress field
Cell	Agent-based	Cell shape, focal adhesions
Molecular	Rate equations	Channel states, signaling

8.8.2 Coupling Strategy

1. Solve tissue-level mechanics (stress distribution)
2. Interpolate stress to cell positions
3. Update channel open probabilities
4. Compute calcium/signaling dynamics
5. Update cell phenotype based on signaling
6. Feedback: cell forces modify tissue mechanics

8.8.3 MesoBio Implementation

The framework includes:

- Piezo channel gating models
- Calcium dynamics ODEs
- YAP/TAZ nuclear translocation
- Coupling to LBM fluid solver

8.9 Channel Capacity of Mechanotransduction

8.9.1 Information-Theoretic View

From Chapter 3, mechanotransduction channels transmit limited information:

$$I(\sigma; R) = H(R) - H(R|\sigma) \lesssim 2 \text{ bits} \tag{8.12}$$

This explains:

- Why cells use multiple mechanosensors
- Why response thresholds exist
- Why adaptation is essential

8.9.2 Implications for Modeling

Models should not assume continuous stress-response relationships. Instead:

- Threshold-based activation
- Discrete signaling states
- Noise and stochasticity important

8.10 Pathological Mechanotransduction

8.10.1 Atherosclerosis

Low and oscillatory shear stress leads to:

- Endothelial dysfunction
- Inflammatory gene expression
- Reduced NO production
- Plaque formation

8.10.2 Cancer Mechanobiology

Tumors exhibit:

- Stiff ECM (up to 10× normal)
- Elevated interstitial pressure
- YAP/TAZ activation promoting proliferation
- Piezo1 upregulation in some cancers

8.10.3 Fibrosis

Progressive stiffening creates positive feedback:

$$\text{Stiff ECM} \rightarrow \text{Myofibroblast activation} \rightarrow \text{More ECM} \rightarrow \text{Stiffer ECM} \tag{8.13}$$

8.11 Experimental Techniques

8.11.1 Mechanical Stimulation Methods

Method	**Stimulus**	**Control**
Flow chamber	Shear stress	Precise shear
Stretch device	Uniaxial/biaxial strain	Strain magnitude/rate
AFM indentation	Local force	pN–nN resolution
Magnetic tweezers	Localized pulling	Bead-receptor specific
Substrate stiffness	Stiffness gradient	Spatial control

8.11.2 Readouts

- Calcium imaging (Fura-2, GCaMP)
- YAP immunofluorescence
- Gene expression (qPCR, RNA-seq)
- Traction force microscopy
- Electrophysiology (patch clamp)

8.12 Summary

Key Concepts

- **Piezo channels** are primary mechanosensitive ion channels; gating follows sigmoidal tension dependence
- **Calcium signaling** couples mechanical forces to downstream responses
- **YAP/TAZ** translocate to nucleus on stiff substrates, promoting proliferation
- **Shear stress sensing** involves glycocalyx, cilia, and junctional complexes
- **Focal adhesions** transmit forces and grow under tension
- **Channel capacity** limits information transmission ($\sim$1–2 bits)

8.13 Further Reading

1. Coste, B. et al. (2010). "Piezo1 and Piezo2 are essential components of distinct mechanically activated cation channels." *Science*.
2. Dupont, S. et al. (2011). "Role of YAP/TAZ in mechanotransduction." *Nature*.
3. Tzima, E. et al. (2005). "A mechanosensory complex that mediates the endothelial cell response to fluid shear stress." *Nature*.
4. Iskratsch, T. et al. (2014). "Appreciating force and shape." *Nature Reviews Molecular Cell Biology*.

Part III

Computational Methods for Mesoscale Biology

Chapter 9

Lattice Boltzmann Methods

9.1 Introduction

The Lattice Boltzmann Method (LBM) has emerged as a powerful alternative to traditional CFD for biological flows. Key advantages:

- Natural handling of complex geometries
- Excellent parallelization on GPUs
- Straightforward boundary conditions
- Extension to multiphase/multicomponent flows
- Coupling with agent-based models

9.2 From Boltzmann to Lattice Boltzmann

9.2.1 The Boltzmann Equation

The continuous Boltzmann equation describes particle distributions:

$$\frac{\partial f}{\partial t} + \mathbf{v} \cdot \boldsymbol{\nabla} f = \Omega(f) \tag{9.1}$$

where:

- $f(\mathbf{x}, \mathbf{v}, t)$ = particle distribution function
- $\mathbf{v}$ = microscopic velocity
- $\Omega(f)$ = collision operator

9.2.2 Discretization Philosophy

LBM discretizes:

1. **Space**: Regular lattice with spacing Δx
2. **Time**: Discrete steps Δt
3. **Velocity**: Finite set $\{\mathbf{c}_i\}_{i=0}^{q-1}$

Result: Distribution functions $f_i(\mathbf{x}, t)$ for each velocity direction.

9.3 Common Lattice Configurations

9.3.1 D2Q9 Lattice (2D)

Nine velocities including rest:

$$\mathbf{c}_i = \begin{cases} (0,0) & i = 0 \\ (\pm 1, 0), (0, \pm 1) & i = 1,2,3,4 \\ (\pm 1, \pm 1) & i = 5,6,7,8 \end{cases} \tag{9.2}$$

Weights:

$$w_i = \begin{cases} 4/9 & i = 0 \\ 1/9 & i = 1,2,3,4 \\ 1/36 & i = 5,6,7,8 \end{cases} \tag{9.3}$$

9.3.2 D3Q19 Lattice (3D)

Nineteen velocities for 3D flows:

- 1 rest velocity: $(0, 0, 0)$
- 6 face velocities: $(\pm 1, 0, 0)$, $(0, \pm 1, 0)$, $(0, 0, \pm 1)$
- 12 edge velocities: $(\pm 1, \pm 1, 0)$, $(\pm 1, 0, \pm 1)$, $(0, \pm 1, \pm 1)$

9.3.3 D3Q27 Lattice (3D)

Twenty-seven velocities (more isotropic but computationally expensive):

- All combinations of $\{-1, 0, 1\}^3$

9.4 The BGK Collision Operator

9.4.1 Single Relaxation Time

The Bhatnagar-Gross-Krook (BGK) approximation:

$$\Omega_i = -\frac{1}{\tau}(f_i - f_i^{eq}) \tag{9.4}$$

The distribution relaxes toward equilibrium with time scale τ.

9.4.2 Equilibrium Distribution

For incompressible flows, the equilibrium is:

$$\boxed{f_i^{eq} = w_i \rho \left[1 + \frac{\mathbf{c}_i \cdot \mathbf{u}}{c_s^2} + \frac{(\mathbf{c}_i \cdot \mathbf{u})^2}{2c_s^4} - \frac{\mathbf{u} \cdot \mathbf{u}}{2c_s^2} \right]} \tag{9.5}$$

where:

- $c_s = c/\sqrt{3}$ is the lattice sound speed
- $c = \Delta x / \Delta t$ is the lattice velocity

9.5 The LBM Algorithm

9.5.1 Stream and Collide

The fundamental LBM update:

$$f_i(\mathbf{x} + \mathbf{c}_i \Delta t, t + \Delta t) = f_i(\mathbf{x}, t) - \frac{\Delta t}{\tau}(f_i - f_i^{eq}) \tag{9.6}$$

9.5.2 Algorithm Steps

1. **Collision**: Compute post-collision distribution

$$f_i^* = f_i - \frac{1}{\tau}(f_i - f_i^{eq}) \tag{9.7}$$

2. **Streaming**: Propagate to neighboring nodes

$$f_i(\mathbf{x} + \mathbf{c}_i, t + 1) = f_i^*(\mathbf{x}, t) \tag{9.8}$$

3. **Macroscopic quantities**: Compute density and velocity

$$\rho = \sum_i f_i \tag{9.9}$$

$$\rho \mathbf{u} = \sum_i f_i \mathbf{c}_i \tag{9.10}$$

9.6 Chapman-Enskog Analysis

9.6.1 Recovery of Navier-Stokes

Through multi-scale expansion, LBM recovers the incompressible Navier-Stokes equations:

$$\partial_t \rho + \boldsymbol{\nabla} \cdot (\rho \mathbf{u}) = 0 \tag{9.11}$$

$$\partial_t (\rho \mathbf{u}) + \boldsymbol{\nabla} \cdot (\rho \mathbf{u}\mathbf{u}) = -\boldsymbol{\nabla} p + \nu \nabla^2 (\rho \mathbf{u}) \tag{9.12}$$

9.6.2 Kinematic Viscosity

The viscosity relates to relaxation time:

$$\boxed{\nu = c_s^2 \left(\tau - \frac{1}{2}\right) \Delta t} \tag{9.13}$$

For stability: $\tau > 0.5$.

9.7 Boundary Conditions

9.7.1 Bounce-Back (No-Slip)

At solid walls, populations reflect:

$$f_{\bar{i}}(\mathbf{x}_b, t + 1) = f_i^*(\mathbf{x}_b, t) \tag{9.14}$$

where $\bar{i}$ denotes the opposite direction to i.

9.7.2 Zou-He Boundary Conditions

For specified velocity at inlet/outlet:

- Use known velocities to determine unknown populations
- Ensures correct mass and momentum flux

9.7.3 Regularized Boundary Conditions

Improved stability by reconstructing non-equilibrium part:

$$f_i = f_i^{eq} + f_i^{(1)} \tag{9.15}$$

where $f_i^{(1)}$ is computed from the stress tensor.

9.7.4 Pressure Boundary Conditions

For specified pressure (density):

$$\rho = \rho_{\text{specified}}, \quad \mathbf{u} = \text{extrapolated} \tag{9.16}$$

9.8 LBM for Non-Newtonian Fluids

9.8.1 Generalized Newtonian Fluids

For shear-thinning/thickening fluids:

$$\tau(\mathbf{x}, t) = \frac{1}{2} + \frac{\nu(\dot{\gamma})}{c_s^2 \Delta t} \tag{9.17}$$

where $\nu(\dot{\gamma})$ is the local viscosity from constitutive model.

9.8.2 Implementation

1. Compute strain rate tensor from non-equilibrium distributions:

$$\Pi_{\alpha\beta}^{neq} = \sum_i f_i^{neq} c_{i\alpha} c_{i\beta} \tag{9.18}$$

2. Calculate shear rate:

$$\dot{\gamma} = \sqrt{2\boldsymbol{D} : \boldsymbol{D}} \tag{9.19}$$

3. Update local viscosity (e.g., Carreau-Yasuda)
4. Update local relaxation time

9.8.3 Carreau-Yasuda in LBM

$$\nu(\dot{\gamma}) = \nu_\infty + (\nu_0 - \nu_\infty)[1 + (\lambda\dot{\gamma})^a]^{(n-1)/a} \tag{9.20}$$

9.9 LBM for Porous Media

9.9.1 Brinkman-LBM

Add drag force for porous media:

$$\mathbf{f}_{\text{porous}} = -\frac{\nu\varepsilon}{K}\mathbf{u} \tag{9.21}$$

Implemented through forcing term in LBM.

9.9.2 Forchheimer Correction

For higher Reynolds number porous flow:

$$\mathbf{f} = -\frac{\nu\varepsilon}{K}\mathbf{u} - \frac{\varepsilon^2 C_F}{\sqrt{K}}|\mathbf{u}|\mathbf{u} \tag{9.22}$$

9.10 Forcing Terms

9.10.1 Body Forces

External forces (gravity, pressure gradient):

$$f_i^* = f_i - \frac{1}{\tau}(f_i - f_i^{eq}) + \Delta t \cdot F_i \tag{9.23}$$

Common forcing schemes:

- Guo forcing (second-order accurate)
- Exact difference method
- He-Shan-Doolen

9.10.2 Guo Forcing

$$F_i = w_i \left(1 - \frac{1}{2\tau}\right)\left[\frac{\mathbf{c}_i - \mathbf{u}}{c_s^2} + \frac{(\mathbf{c}_i \cdot \mathbf{u})}{c_s^4}\mathbf{c}_i\right] \cdot \mathbf{f} \tag{9.24}$$

This ensures correct momentum:

$$\rho\mathbf{u} = \sum_i f_i \mathbf{c}_i + \frac{\Delta t}{2}\mathbf{f} \tag{9.25}$$

9.11 Multi-Relaxation Time (MRT)

9.11.1 Motivation

BGK has limitations:

- Single relaxation time for all modes
- Limited stability at low viscosity
- Boundary condition accuracy issues

9.11.2 MRT Formulation

Transform to moment space:

$$\mathbf{m} = \boldsymbol{M}\mathbf{f} \tag{9.26}$$

Collision in moment space:

$$\mathbf{m}^* = \mathbf{m} - \boldsymbol{S}(\mathbf{m} - \mathbf{m}^{eq}) \tag{9.27}$$

where $\boldsymbol{S}$ is diagonal with different relaxation rates for different moments.

9.12 LBM-IBM Coupling

9.12.1 Integration with Immersed Boundary

LBM provides efficient flow solver for IBM:

1. LBM collision and streaming
2. Interpolate velocity to Lagrangian points
3. Compute boundary forces
4. Spread forces to Eulerian grid
5. Add forces to LBM via Guo forcing
6. Update Lagrangian positions

9.12.2 Advantages

- Both methods work on regular grids
- Local operations—excellent GPU performance
- Natural coupling through force spreading

9.13 GPU Implementation

9.13.1 Memory Layout

Two common approaches:

- **Structure of Arrays (SoA)**: f_i[all nodes] — better memory coalescing
- **Array of Structures (AoS)**: node[$f_0, f_1, \ldots$] — simpler indexing

9.13.2 Kernel Design

```
# JAX/GPU-optimized LBM collision kernel
@jax.jit
def collision_kernel(f, rho, u, tau):
    # Compute equilibrium (vectorized)
    cu = jnp.einsum('xyc,qc->xyq', u, c)
    usq = jnp.sum(u**2, axis=-1, keepdims=True)
    feq = w * rho[..., None] * (
        1 + cu/cs2 + cu**2/(2*cs4) - usq/(2*cs2)
    )
    # BGK collision
    return f - (f - feq) / tau
```

9.13.3 Performance Considerations

- Minimize CPU-GPU transfers
- Fuse collision and streaming when possible
- Use single precision for non-critical calculations
- Consider AA-pattern for reduced memory

9.14 Advection-Diffusion LBM

9.14.1 Passive Scalar Transport

Separate distribution g_i for concentration:

$$g_i(\mathbf{x} + \mathbf{c}_i, t + 1) = g_i - \frac{1}{\tau_g}(g_i - g_i^{eq}) \tag{9.28}$$

with equilibrium:

$$g_i^{eq} = w_i C \left(1 + \frac{\mathbf{c}_i \cdot \mathbf{u}}{c_s^2}\right) \tag{9.29}$$

Diffusion coefficient:

$$D = c_s^2 \left(\tau_g - \frac{1}{2}\right) \Delta t \tag{9.30}$$

9.15 Validation

9.15.1 Analytical Solutions

Test cases with known solutions:

- Poiseuille flow (parabolic profile)
- Couette flow (linear profile)
- Womersley flow (pulsatile, Bessel functions)
- Decay of Taylor-Green vortex

9.15.2 Benchmark: Lid-Driven Cavity

Standard 2D benchmark:

- Compare velocity profiles at centerlines
- Ghia et al. (1982) reference data
- Re = 100, 400, 1000 typical test cases

9.16 Applications in Biology

9.16.1 Perivascular Space Flow

LBM captures:

- Pulsatile flow from arterial wall motion
- Low Reynolds number (Re $\sim 10^{-2}$)
- Complex annular geometry

9.16.2 Blood Flow in Microcirculation

With non-Newtonian extension:

- Shear-thinning blood rheology
- RBC deformation (IBM coupling)
- Plasma skimming effects

9.16.3 Intestinal Flow

Modeling:

- Peristaltic contractions via IBM
- Mixing enhancement by villi
- Mass transfer in unstirred layer

9.17 Summary

Key Concepts

- **LBM** evolves distribution functions through stream-collide dynamics
- **BGK collision** relaxes toward equilibrium with rate $1/\tau$
- **Viscosity** $\nu = c_s^2(\tau - 1/2)\Delta t$ from Chapman-Enskog
- **Bounce-back** implements no-slip boundaries
- **Non-Newtonian**: Local τ from shear-rate-dependent viscosity
- **GPU acceleration** through parallelizable local operations

9.18 Further Reading

1. Succi, S. (2018). *The Lattice Boltzmann Equation: For Complex States of Flowing Matter*. Oxford.
2. Krüger, T. et al. (2017). *The Lattice Boltzmann Method: Principles and Practice*. Springer.
3. Aidun, C.K. & Clausen, J.R. (2010). "Lattice-Boltzmann Method for Complex Flows." *Annual Review of Fluid Mechanics*.
4. Guo, Z. & Shu, C. (2013). *Lattice Boltzmann Method and Its Applications in Engineering*. World Scientific.

Chapter 10

Agent-Based Modeling of Cells

10.1 Introduction to Agent-Based Models

Agent-based models (ABMs) represent biological systems as collections of discrete entities (agents) that interact according to defined rules. For cell biology:

- Each cell is an agent with state variables
- Cells interact with neighbors and environment
- Emergent tissue-level behavior from local rules
- Natural representation of cell heterogeneity

10.2 Why Agent-Based Modeling?

10.2.1 Advantages over Continuum Models

Aspect	**Continuum**	**Agent-Based**
Cell individuality	Averaged	Preserved
Heterogeneity	Difficult	Natural
Discrete events	Approximated	Exact
Stochasticity	Added noise	Intrinsic
Spatial resolution	Grid-limited	Arbitrary

10.2.2 When to Use ABM

ABMs are preferred when:

- Cell-cell interactions are important
- Population heterogeneity matters
- Discrete events (division, death) are key
- Cell number is tractable (10^2–10^6 cells)

10.3 Cell State Variables

10.3.1 Geometric Properties

Property	Symbol	Typical Values
Position	$\mathbf{x}$	Coordinates in domain
Volume	V	500–5000 μm^3
Radius (spherical)	R	5–15 μm
Nuclear radius	R_n	3–8 μm
Surface area	A	300–3000 μm^2

10.3.2 Phenotypic Properties

- **Cell cycle phase**: G0, G1, S, G2, M
- **Cell type**: Epithelial, endothelial, immune, etc.
- **Differentiation state**: Stem, progenitor, differentiated
- **Metabolic state**: Normoxic, hypoxic, necrotic

10.3.3 Internal Variables

- ATP concentration
- Oxygen level (intracellular)
- Signaling molecule concentrations
- Gene expression states

10.4 Cell Mechanics

10.4.1 Overlapping Spheres Model

Cells as soft spheres with repulsion when overlapping:

$$F_{ij}^{\text{rep}} = \begin{cases} k_r(d_{ij} - r_i - r_j)\hat{\mathbf{n}}_{ij} & \text{if } d_{ij} < r_i + r_j \\ 0 & \text{otherwise} \end{cases} \tag{10.1}$$

where d_{ij} is center-to-center distance and $\hat{\mathbf{n}}_{ij}$ is the unit normal.

10.4.2 Adhesion Forces

Cell-cell adhesion (simplified):

$$F_{ij}^{\text{adh}} = \begin{cases} k_a(d_{ij} - d_0)\hat{\mathbf{n}}_{ij} & \text{if } d_0 < d_{ij} < d_{\max} \\ 0 & \text{otherwise} \end{cases} \tag{10.2}$$

where d_0 is the equilibrium separation.

10.4.3 Johnson-Kendall-Roberts (JKR) Theory

More accurate contact mechanics including adhesion:

$$F = \frac{4E^*}{3R^*}a^3 - \sqrt{8\pi\gamma E^* a^3} \tag{10.3}$$

where:

- a = contact radius
- E^* = effective elastic modulus
- R^* = effective radius
- γ = surface energy

10.4.4 Equation of Motion

Overdamped dynamics (low Reynolds number):

$$\eta\frac{d\mathbf{x}_i}{dt} = \sum_j \mathbf{F}_{ij} + \mathbf{F}_i^{\text{ext}} + \mathbf{F}_i^{\text{random}} \tag{10.4}$$

where η is the damping coefficient (related to viscous medium).

10.5 Cell Proliferation

10.5.1 Cell Cycle Model

Cells progress through phases with transition rates:

$$\text{G1} \xrightarrow{k_{G1\to S}} \text{S} \xrightarrow{k_{S\to G2}} \text{G2} \xrightarrow{k_{G2\to M}} \text{M} \xrightarrow{k_{\text{div}}} 2\ \text{G1 cells} \tag{10.5}$$

10.5.2 Transition Rates

Rates depend on environment:

$$k_{G1\to S} = k^0_{G1\to S} \cdot f(\text{O}_2) \cdot g(\text{nutrients}) \cdot h(\text{signals}) \tag{10.6}$$

Example oxygen dependence:

$$f(\text{O}_2) = \frac{[\text{O}_2]}{[\text{O}_2] + K_{\text{O}_2}} \tag{10.7}$$

10.5.3 Volume Growth

During interphase, cell volume increases:

$$\frac{dV}{dt} = k_{\text{growth}} \cdot (V_{\text{target}} - V) \tag{10.8}$$

Division occurs when $V \geq 2V_0$ or phase timer expires.

10.6 Cell Death

10.6.1 Apoptosis (Programmed Death)

Triggered by:

- Death ligand signaling (FasL, TRAIL)
- DNA damage (p53 pathway)
- Growth factor withdrawal
- Mechanical stress

Model:

$$P_{\text{apoptosis}} = 1 - \exp(-k_{\text{apo}} \cdot \Delta t) \tag{10.9}$$

10.6.2 Necrosis

Uncontrolled death from:

- Severe hypoxia ($[O_2] < [O_2]_{\text{crit}}$)
- ATP depletion
- Extreme mechanical damage

10.6.3 Death Process

Dying cells may:

- Shrink (apoptosis)
- Swell and lyse (necrosis)
- Release signals (damage-associated molecular patterns)
- Be removed by phagocytosis

10.7 Cell Migration

10.7.1 Random Motility

Persistent random walk:

$$\mathbf{v}(t + \Delta t) = (1 - \lambda \Delta t)\mathbf{v}(t) + \sqrt{2D_r \Delta t}\boldsymbol{\xi} \tag{10.10}$$

where:

- λ = persistence time inverse
- D_r = rotational diffusion coefficient
- $\boldsymbol{\xi}$ = unit random vector

Mean squared displacement:

$$\langle r^2(t) \rangle = 2nD_{\text{eff}}t + \frac{v_0^2}{\lambda^2}(e^{-\lambda t} + \lambda t - 1) \tag{10.11}$$

10.7.2 Chemotaxis

Migration up concentration gradient:

$$\mathbf{v}_{\text{chem}} = \chi \frac{\boldsymbol{\nabla} C}{|C|} \cdot f(C) \tag{10.12}$$

where χ is the chemotactic coefficient and $f(C)$ models receptor saturation.

10.7.3 Haptotaxis

Migration along ECM adhesion gradients:

$$\mathbf{v}_{\text{hapto}} = \kappa \boldsymbol{\nabla} \rho_{\text{ECM}} \tag{10.13}$$

10.7.4 Durotaxis

Migration toward stiffer substrates:

$$\mathbf{v}_{\text{duro}} = \xi \boldsymbol{\nabla} E_{\text{substrate}} \tag{10.14}$$

10.8 Intracellular Dynamics

10.8.1 ODE-Based Models

Simple signaling networks:

$$\frac{d[X]}{dt} = k_{\text{prod}} - k_{\text{deg}}[X] + (\text{reactions}) \tag{10.15}$$

10.8.2 Example: Hypoxia Response

HIF-1α stabilization under hypoxia:

$$\frac{d[\text{HIF}]}{dt} = k_{\text{syn}} - k_{\text{deg}}([\text{O}_2])[\text{HIF}] \tag{10.16}$$

with:

$$k_{\text{deg}}([\text{O}_2]) = k_{\text{deg}}^0 \cdot \frac{[\text{O}_2]}{[\text{O}_2] + K_m} \tag{10.17}$$

10.8.3 Coupling to Phenotype

Intracellular states determine behavior:

$$[\text{HIF}] > \text{threshold} \implies \text{switch to glycolytic metabolism} \tag{10.18}$$

10.9 Phenotype State Machines

10.9.1 Discrete States

Cells occupy discrete phenotypic states:

- Proliferating
- Quiescent (G0)
- Migrating
- Apoptotic
- Necrotic

10.9.2 Transition Rules

State transitions based on conditions:

```
if oxygen < hypoxia_threshold:
    if oxygen < necrosis_threshold:
        cell.state = NECROTIC
    else:
        cell.state = QUIESCENT
elif pressure > pressure_threshold:
    cell.state = QUIESCENT  # Contact inhibition
else:
    cell.state = PROLIFERATING
```

10.10 Software Frameworks

10.10.1 PhysiCell

Open-source framework for agent-based tumor modeling:

- C++ with parallelization
- BioFVM for diffusion solver
- PhysiBoSS for Boolean networks
- XML configuration

10.10.2 CompuCell3D

Cellular Potts Model framework:

- Python + C++
- Energy-based cell mechanics
- Natural for cell shape modeling
- Plugin architecture

10.10.3 Chaste

Oxford framework for cardiac/cancer modeling:

- C++ with Python bindings
- Multiple cell models (center-based, vertex)
- PDE coupling
- Extensive testing framework

10.11 Coupling to Microenvironment

10.11.1 Field Variables

The microenvironment contains:

- Oxygen concentration
- Nutrient levels (glucose, glutamine)
- Growth factors (EGF, VEGF)
- Waste products (lactate, H^+)
- ECM density

10.11.2 Cell Uptake/Secretion

Mass balance:

$$\frac{\partial C}{\partial t} = D\nabla^2 C - \sum_{\text{cells}} q_i \delta(\mathbf{x} - \mathbf{x}_i) \tag{10.19}$$

where q_i is the uptake/secretion rate of cell i.

10.11.3 Uptake Models

Michaelis-Menten uptake:

$$q = q_{\max} \frac{C}{K_m + C} \tag{10.20}$$

10.12 Computational Considerations

10.12.1 Time Stepping

Multiple time scales require care:

Process	Time Scale
Mechanics update	0.01–0.1 min
Diffusion	0.1–1 min
Phenotype decisions	1–10 min
Cell cycle	hours

10.12.2 Neighbor Finding

Efficient search using:

- Cell lists (grid-based binning)
- Verlet lists (neighbor caching)
- kd-trees for sparse distributions

10.12.3 Parallelization

Strategies:

- OpenMP for shared memory
- Domain decomposition for distributed
- GPU acceleration for mechanics/diffusion

10.13 Model Calibration and Validation

10.13.1 Parameter Sources

Parameter	Source	Method
Cell radius	Imaging	Direct measurement
Doubling time	Culture	Growth curves
Migration speed	Tracking	Mean displacement
Oxygen consumption	Respirometry	Seahorse assay
Adhesion strength	AFM	Force spectroscopy

10.13.2 Emergent Validation

Compare model predictions to experiments:

- Spheroid growth kinetics
- Invasion front speed
- Spatial patterns (necrotic core)
- Response to perturbations

10.14 Example: Tumor Spheroid

10.14.1 Setup

```
# Initialize tumor spheroid
for i in range(n_cells):
    x = random_in_sphere(R_initial)
    cell = Cell(
        position=x,
        radius=5.0,  # microns
        cycle_phase='G1',
        o2_uptake=10.0  # amol/cell/min
    )
    cells.append(cell)
```

10.14.2 Emergent Behavior

Simulations reproduce:

- Oxygen gradient (high periphery, low core)
- Proliferating rim

- Quiescent intermediate zone
- Necrotic core (if large enough)
- Gompertzian growth kinetics

10.15 Summary

Key Concepts

- **ABMs** represent cells as discrete agents with state and rules
- **Cell mechanics** through overlapping spheres or JKR contact models
- **Cell cycle** progression with environment-dependent rates
- **Phenotype transitions** via discrete state machines
- **Microenvironment coupling** through uptake/secretion source terms
- Frameworks: **PhysiCell**, CompuCell3D, Chaste

10.16 Further Reading

1. Ghaffarizadeh, A. et al. (2018). "PhysiCell: An open source physics-based cell simulator." *PLoS Computational Biology.*
2. Swat, M.H. et al. (2012). "Multi-scale modeling of tissues using CompuCell3D." *Methods in Cell Biology.*
3. Macklin, P. et al. (2012). "Patient-calibrated agent-based modelling of ductal carcinoma." *Journal of Theoretical Biology.*
4. Anderson, A.R.A. & Quaranta, V. (2008). "Integrative mathematical oncology." *Nature Reviews Cancer.*

Chapter 11

Continuum-Discrete Coupling

11.1 The Multi-Scale Challenge

Biological systems exhibit phenomena across scales:

Scale	Model Type	Physics
nm–μm	Molecular dynamics	Protein interactions
μm–mm	Agent-based	Cell mechanics
mm–cm	Continuum	Tissue flow/mechanics

The mesoscale requires coupling agent-based cell models with continuum descriptions of the microenvironment.

11.2 Eulerian-Lagrangian Framework

11.2.1 Dual Representation

- **Eulerian (continuum)**: Field variables on fixed grid
  - Concentration fields $C(\mathbf{x}, t)$
  - Velocity field $\mathbf{u}(\mathbf{x}, t)$
  - Pressure $p(\mathbf{x}, t)$
- **Lagrangian (discrete)**: Agent properties
  - Cell positions $\mathbf{X}_i(t)$
  - Cell states $\sigma_i(t)$
  - Cell-local concentrations

11.2.2 Coupling Operators

Two fundamental operations:

1. **Interpolation** $\mathcal{I}$: Field $\to$ Agent

$$C_i = \mathcal{I}[C](\mathbf{X}_i) = \int C(\mathbf{x})\delta(\mathbf{x} - \mathbf{X}_i)d\mathbf{x} \tag{11.1}$$

2. **Spreading** $\mathcal{S}$: Agent $\to$ Field

$$S(\mathbf{x}) = \mathcal{S}[\{q_i\}] = \sum_i q_i \delta(\mathbf{x} - \mathbf{X}_i) \tag{11.2}$$

11.3 Interpolation Methods

11.3.1 Nearest Grid Point (NGP)

Simplest approach:

$$C_i = C(\mathbf{x}_{\text{nearest to } \mathbf{X}_i}) \tag{11.3}$$

Pros: Fast, simple. Cons: First-order, noisy.

11.3.2 Cloud-in-Cell (CIC) / Bilinear

Linear interpolation using surrounding nodes:

$$C_i = \sum_{j \in \text{neighbors}} w_j C_j \tag{11.4}$$

For 2D with cell at (x_p, y_p) in grid cell (i, j) to $(i+1, j+1)$:

$$w_{00} = (1-\xi)(1-\eta) \tag{11.5}$$
$$w_{10} = \xi(1-\eta) \tag{11.6}$$
$$w_{01} = (1-\xi)\eta \tag{11.7}$$
$$w_{11} = \xi\eta \tag{11.8}$$

where $\xi = (x_p - x_i)/\Delta x$, $\eta = (y_p - y_j)/\Delta y$.

11.3.3 Higher-Order Interpolation

Cubic splines for smoother interpolation:

$$C_i = \sum_j W(|\mathbf{X}_i - \mathbf{x}_j|/h) C_j \tag{11.9}$$

Common kernels:

- Triangular shaped cloud (TSC): 2nd order
- Piecewise cubic spline (PCS): 3rd order
- M4 kernel: 4th order

11.4 Spreading Methods

11.4.1 Cell-Averaged Sources

Agent contribution distributed to nearby nodes:

$$S_j = \frac{1}{\Delta V} \sum_i q_i W(|\mathbf{x}_j - \mathbf{X}_i|/h) \tag{11.10}$$

11.4.2 Regularized Delta Functions

Same kernels as immersed boundary:

$$S(\mathbf{x}) = \sum_i q_i \phi_h(\mathbf{x} - \mathbf{X}_i) \tag{11.11}$$

with ϕ_h the regularized delta function (Chapter 7).

11.4.3 Conservation Properties

For physical consistency:

- Total mass conserved: $\int S\,dV = \sum_i q_i$
- Interpolation and spreading should be adjoint

11.5 Time Integration Strategies

11.5.1 The Multi-Rate Problem

Different components evolve at different rates:

Process	Time Scale	CFL/Stability
LBM fluid	μs–ms	$\Delta t < \Delta x/c_s$
Diffusion	ms–s	$\Delta t < \Delta x^2/2D$
Cell mechanics	s–min	$\Delta t < \sqrt{m/k}$
Phenotype update	min–h	Biological rates

11.5.2 Subcycling

Fast physics takes multiple steps per slow physics step:

```
for t in range(n_steps):
    # Slow update (cells)
    update_cell_phenotypes(cells, dt_cell)

    # Fast subcycling (fluid, diffusion)
    for sub in range(n_sub):
        lbm_step(dt_fluid)
        diffusion_step(dt_fluid)

    # Coupling
    interpolate_fields_to_cells()
    spread_cell_sources()
```

11.5.3 Operator Splitting

Separate physics into sequential steps:

$$\mathcal{L} = \mathcal{L}_{\text{advection}} + \mathcal{L}_{\text{diffusion}} + \mathcal{L}_{\text{reaction}} + \mathcal{L}_{\text{cells}} \tag{11.12}$$

First-order (Lie) splitting:

$$y^{n+1} = e^{\mathcal{L}_4\Delta t} e^{\mathcal{L}_3\Delta t} e^{\mathcal{L}_2\Delta t} e^{\mathcal{L}_1\Delta t} y^n \tag{11.13}$$

Second-order (Strang) splitting:

$$y^{n+1} = e^{\mathcal{L}_1\Delta t/2} e^{\mathcal{L}_2\Delta t/2} \cdots e^{\mathcal{L}_2\Delta t/2} e^{\mathcal{L}_1\Delta t/2} y^n \tag{11.14}$$

11.6 Source Term Implementation

11.6.1 Uptake by Cells

Cells consume nutrients:

$$\frac{\partial C}{\partial t} = D\nabla^2 C - \sum_i q_i(\mathbf{X}_i, C)\phi_h(\mathbf{x} - \mathbf{X}_i) \tag{11.15}$$

11.6.2 Secretion by Cells

Cells release factors:

$$\frac{\partial C}{\partial t} = D\nabla^2 C - kC + \sum_i s_i(\mathbf{X}_i)\phi_h(\mathbf{x} - \mathbf{X}_i) \tag{11.16}$$

11.6.3 Implementation Notes

- Pre-compute spreading weights for efficiency
- Use cell lists for localized spreading
- Handle boundary cells carefully

11.7 Feedback Mechanisms

11.7.1 Mechanical Feedback

Cell motion affects fluid flow:

$$\mathbf{f}(\mathbf{x}) = \sum_i \mathbf{F}_i^{\text{drag}} \phi_h(\mathbf{x} - \mathbf{X}_i) \tag{11.17}$$

11.7.2 Chemical Feedback

Cell state affects secretion:

$$s_i = s_0 \cdot f(\text{cell phenotype}) \cdot g(C_{\text{local}}) \tag{11.18}$$

Example: Hypoxic cells secrete VEGF:

$$s_{\text{VEGF}} = s_{\max} \cdot \frac{K_{\text{O}_2}^n}{K_{\text{O}_2}^n + [\text{O}_2]^n} \tag{11.19}$$

11.7.3 Mechanotransduction Feedback

From Chapter 8, mechanical stress affects cell behavior:

$$\text{stress field} \xrightarrow{\mathcal{I}} \text{cell stress} \to \text{Piezo/YAP} \to \text{phenotype} \tag{11.20}$$

11.8 Software Architecture

11.8.1 Modular Design

```
class HybridSimulator:
    def __init__(self):
        self.fluid_solver = LBMSolver()
        self.diffusion_solver = ADRSolver()
        self.cell_population = CellPopulation()
        self.coupler = Coupler()

    def step(self, dt):
        # Update continuum fields
        self.fluid_solver.step(dt_fluid, n_sub)
        self.diffusion_solver.step(dt_diff, n_sub)
```

```
        # Coupling: field -> agents
        self.coupler.interpolate(
            self.diffusion_solver.fields,
            self.cell_population
        )

        # Update agents
        self.cell_population.update(dt)

        # Coupling: agents -> field
        self.coupler.spread(
            self.cell_population,
            self.diffusion_solver.sources
        )
```

11.8.2 Data Structures

Field representation:

```
class Field:
    def __init__(self, nx, ny, nz):
        self.data = backend.zeros((nx, ny, nz))
        self.dx = domain_size / nx
        self.origin = (0, 0, 0)

    def interpolate(self, position):
        # Return value at arbitrary position
        ...

    def add_source(self, position, value, kernel):
        # Spread point source to grid
        ...
```

11.8.3 Parallel Considerations

Domain decomposition challenges:

- Cells can migrate between domains
- Ghost cells for boundary coupling
- Load imbalance as cells cluster

Solutions:

- Dynamic load balancing
- Overlapping partitions
- Cell-centered decomposition

11.9 Example: Tumor Growth

11.9.1 Model Components

1. **Oxygen diffusion**:

$$\frac{\partial [\mathrm{O}_2]}{\partial t} = D_{\mathrm{O}_2} \nabla^2 [\mathrm{O}_2] - \sum_i q_i^{\mathrm{O}_2} \phi_h \tag{11.21}$$

2. **VEGF diffusion**:

$$\frac{\partial[\text{VEGF}]}{\partial t} = D_{\text{VEGF}}\nabla^2[\text{VEGF}] - k[\text{VEGF}] + \sum_i s_i^{\text{VEGF}}\phi_h \tag{11.22}$$

3. **Cell agents**: Position, volume, cycle phase, O_2 uptake
4. **Coupling**: $O_2 \rightarrow$ cell proliferation; hypoxia $\rightarrow$ VEGF secretion

11.9.2 Algorithm

1. Initialize tumor seed cells and oxygen field
2. Loop:
   (a) Solve diffusion equations with cell sources
   (b) Interpolate O_2 to cells
   (c) Update cell phenotypes (proliferate/quiesce/die)
   (d) Update cell mechanics (repulsion, adhesion)
   (e) Move cells
   (f) Handle division (add daughter cell)
   (g) Update source terms

11.10 Example: Glymphatic Flow

11.10.1 Model Components

1. **LBM fluid**: Pulsatile perivascular flow
2. **Advection-diffusion**: Aβ transport
3. **Agents**: Astrocyte endfeet (AQP4 polarization)
4. **Coupling**: Wall motion $\rightarrow$ flow $\rightarrow$ clearance

11.10.2 Coupling Points

- IBM: Arterial wall motion drives fluid
- AQP4: Modulates water flux at boundaries
- Solute: Cleared by combined advection + diffusion

11.11 Verification Strategies

11.11.1 Interpolation Accuracy

Test with known smooth field:

$$C(\mathbf{x}) = \sin(k_x x)\sin(k_y y) \tag{11.23}$$

Verify:

- Interpolation converges with grid refinement
- Spreading conserves total mass
- Round-trip (interpolate then spread) errors

11.11.2 Conservation Tests

For closed system:

$$\frac{d}{dt}\left(\int_\Omega C\,dV + \sum_i C_i^{\text{internal}} V_i\right) = 0 \tag{11.24}$$

11.11.3 Method of Manufactured Solutions

Choose solution C_{exact}, compute required source:

$$S = \frac{\partial C_{\text{exact}}}{\partial t} + \mathbf{u}\cdot\boldsymbol{\nabla} C_{\text{exact}} - D\nabla^2 C_{\text{exact}} - R \tag{11.25}$$

Compare numerical solution to C_{exact}.

11.12 Performance Optimization

11.12.1 GPU Acceleration

Continuum solvers parallelize well:

- LBM: Local operations, excellent GPU fit
- Diffusion: Stencil operations, good parallelism

Agent operations more challenging:

- Variable work per cell
- Neighbor searches
- Random number generation

11.12.2 Memory Efficiency

- Sparse fields for localized concentrations
- Compressed storage for inactive regions
- Adaptive mesh refinement near cells

11.12.3 Load Balancing

Cell clustering creates imbalance:

- Space-filling curves for locality
- Dynamic repartitioning
- Hybrid MPI+threads

11.13 Summary

Key Concepts

- **Eulerian-Lagrangian coupling** connects continuum fields to discrete cells
- **Interpolation** maps field values to agent locations
- **Spreading** distributes agent sources to grid
- **Operator splitting** handles multiple time scales
- **Feedback loops** couple cell behavior to environment and vice versa
- **Verification** ensures coupling preserves conservation and accuracy

11.14 Further Reading

1. Macklin, P. et al. (2016). "Computational models of tumor growth." *Annual Review of Biomedical Engineering*.

2. Ghaffarizadeh, A. et al. (2016). "BioFVM: An efficient, parallelized diffusive transport solver." *Bioinformatics*.

3. Hockney, R.W. & Eastwood, J.W. (1988). *Computer Simulation Using Particles*. CRC Press.

4. Quarteroni, A. et al. (2017). *Mathematical Modelling of the Human Cardiovascular System*. Cambridge.

Chapter 12

Numerical Methods and Validation

12.1 Introduction

Computational biology requires rigorous numerical methods and validation strategies. This chapter covers:

- Time integration schemes
- Spatial discretization
- Stability and accuracy analysis
- Verification and validation approaches

12.2 Time Integration

12.2.1 Explicit Methods

Forward Euler:

$$y^{n+1} = y^n + \Delta t \cdot f(y^n, t^n) \tag{12.1}$$

Properties:

- First-order accurate: $\mathcal{O}(\Delta t)$
- Conditionally stable
- Simple, low memory

Runge-Kutta 4 (RK4):

$$k_1 = f(y^n, t^n) \tag{12.2}$$

$$k_2 = f(y^n + \frac{\Delta t}{2} k_1, t^n + \frac{\Delta t}{2}) \tag{12.3}$$

$$k_3 = f(y^n + \frac{\Delta t}{2} k_2, t^n + \frac{\Delta t}{2}) \tag{12.4}$$

$$k_4 = f(y^n + \Delta t \cdot k_3, t^n + \Delta t) \tag{12.5}$$

$$y^{n+1} = y^n + \frac{\Delta t}{6}(k_1 + 2k_2 + 2k_3 + k_4) \tag{12.6}$$

Properties:

- Fourth-order accurate: $\mathcal{O}(\Delta t^4)$
- Conditionally stable
- Four function evaluations per step

12.2.2 Implicit Methods

Backward Euler:

$$y^{n+1} = y^n + \Delta t \cdot f(y^{n+1}, t^{n+1}) \tag{12.7}$$

Properties:

- First-order accurate
- Unconditionally stable (A-stable)
- Requires nonlinear solve

Crank-Nicolson:

$$y^{n+1} = y^n + \frac{\Delta t}{2}\left[f(y^n, t^n) + f(y^{n+1}, t^{n+1})\right] \tag{12.8}$$

Properties:

- Second-order accurate
- A-stable
- Good for diffusion problems

12.2.3 Stability Regions

For the test equation $\frac{dy}{dt} = \lambda y$:

Method	**Stability Condition**
Forward Euler	$\lvert\lambda\Delta t\rvert < 2$ (real $\lambda < 0$)
RK4	$\lvert\lambda\Delta t\rvert \lesssim 2.8$
Backward Euler	Always stable
Crank-Nicolson	Always stable

12.2.4 Stiff Systems

Biological systems often have multiple time scales:

$$\text{Stiffness ratio} = \frac{\max|\lambda_i|}{\min|\lambda_i|} \gg 1 \tag{12.9}$$

For stiff systems, use:

- Implicit methods (backward Euler, BDF)
- Semi-implicit (IMEX) schemes
- Exponential integrators

12.3 Spatial Discretization

12.3.1 Finite Difference Methods

Central differences (second-order):

$$\frac{\partial C}{\partial x} \approx \frac{C_{i+1} - C_{i-1}}{2\Delta x} \tag{12.10}$$

$$\frac{\partial^2 C}{\partial x^2} \approx \frac{C_{i+1} - 2C_i + C_{i-1}}{\Delta x^2} \tag{12.11}$$

Upwind (first-order, for advection):

$$u\frac{\partial C}{\partial x} \approx \begin{cases} u\frac{C_i - C_{i-1}}{\Delta x} & u > 0 \\ u\frac{C_{i+1} - C_i}{\Delta x} & u < 0 \end{cases} \tag{12.12}$$

12.3.2 Advection Schemes

For the advection equation $\frac{\partial C}{\partial t} + u\frac{\partial C}{\partial x} = 0$:

FTCS (unstable!):

$$C_i^{n+1} = C_i^n - \frac{u\Delta t}{2\Delta x}(C_{i+1}^n - C_{i-1}^n) \tag{12.13}$$

Lax-Wendroff (second-order):

$$C_i^{n+1} = C_i^n - \frac{\sigma}{2}(C_{i+1}^n - C_{i-1}^n) + \frac{\sigma^2}{2}(C_{i+1}^n - 2C_i^n + C_{i-1}^n) \tag{12.14}$$

where $\sigma = u\Delta t/\Delta x$ is the CFL number.

MUSCL-Hancock (high resolution):

- Linear reconstruction with limiters
- Prevents spurious oscillations
- Second-order accurate

12.3.3 The CFL Condition

For explicit advection:

$$\text{CFL} = \frac{|u|\Delta t}{\Delta x} \leq 1 \tag{12.15}$$

Physical interpretation: Information cannot travel more than one cell per time step.

12.3.4 Diffusion Stability

For explicit diffusion:

$$\frac{D\Delta t}{\Delta x^2} \leq \frac{1}{2} \quad \text{(1D)} \tag{12.16}$$

$$\frac{D\Delta t}{\Delta x^2} \leq \frac{1}{4} \quad \text{(2D)} \tag{12.17}$$

$$\frac{D\Delta t}{\Delta x^2} \leq \frac{1}{6} \quad \text{(3D)} \tag{12.18}$$

12.4 Error Analysis

12.4.1 Truncation Error

Local error introduced by discretization:

$$\tau = \text{exact operator} - \text{discrete operator} \tag{12.19}$$

For central difference:

$$\frac{\partial^2 C}{\partial x^2} = \frac{C_{i+1} - 2C_i + C_{i-1}}{\Delta x^2} + \mathcal{O}(\Delta x^2) \tag{12.20}$$

12.4.2 Global Error

Accumulated error over simulation:

$$\text{Global error} \sim \text{Truncation error} \times \text{Number of steps} \tag{12.21}$$

For stable schemes, global error $\sim \mathcal{O}(\Delta t^p)$ where p is the order.

12.4.3 Convergence Studies

Verify order of accuracy:

1. Run simulation at resolutions h, $h/2$, $h/4$
2. Compute error norms E_h, $E_{h/2}$, $E_{h/4}$
3. Order $p \approx \log_2(E_h/E_{h/2})$

12.5 Verification vs. Validation

12.5.1 Definitions

Verification: "Solving the equations right"

- Does the code correctly solve the mathematical model?
- Comparison to analytical solutions
- Code-to-code comparisons

Validation: "Solving the right equations"

- Does the model accurately represent reality?
- Comparison to experimental data
- Quantified uncertainty

12.5.2 The V&V Hierarchy

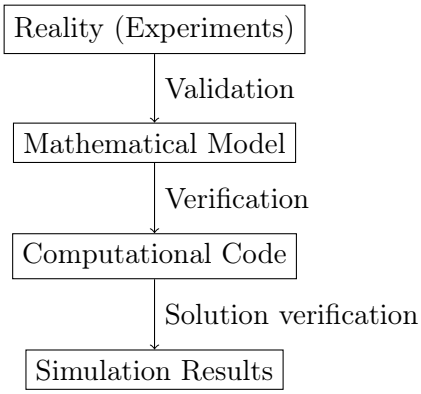

12.6 Method of Manufactured Solutions (MMS)

12.6.1 Concept

Choose a known solution and compute the required source term:

1. Define $C_{\text{exact}}(\mathbf{x}, t)$ (smooth, satisfies BCs)
2. Compute source: $S = \mathcal{L}[C_{\text{exact}}]$
3. Solve with this source term
4. Compare numerical solution to C_{exact}

12.6.2 Example: Advection-Diffusion

Choose:

$$C_{\text{exact}} = \sin(\pi x)\sin(\pi y)\exp(-t) \tag{12.22}$$

Required source:

$$S = -C_{\text{exact}} + u_x \pi \cos(\pi x)\sin(\pi y) + u_y \sin(\pi x)\pi\cos(\pi y) + 2\pi^2 D \cdot C_{\text{exact}} \tag{12.23}$$

12.6.3 Advantages

- Tests full code (not just isolated components)
- Works for any PDE system
- Verifies order of accuracy
- Finds coding errors

12.7 Benchmark Problems

12.7.1 Fluid Mechanics

Lid-Driven Cavity:

- 2D square, top wall moving
- Reference: Ghia et al. (1982)

- Tests Re = 100, 400, 1000, 3200

Poiseuille Flow:

- Channel flow, analytical parabolic profile
- Tests boundary conditions

Taylor-Green Vortex:

- Decaying vortex with analytical solution
- Tests time accuracy

12.7.2 Diffusion

Gaussian Pulse:

$$C(r,t) = \frac{M}{(4\pi Dt)^{n/2}} \exp\left(-\frac{r^2}{4Dt}\right) \tag{12.24}$$

Steady State with Sources:

- Fixed concentration boundaries
- Uniform internal source
- Analytical solution exists

12.7.3 Coupled Systems

Fisher-KPP Equation:

$$\frac{\partial C}{\partial t} = D\nabla^2 C + rC(1-C) \tag{12.25}$$

Traveling wave solution with known speed $v = 2\sqrt{rD}$.

12.8 Error Metrics

12.8.1 Norms

L_1 norm (average error):

$$\|e\|_1 = \frac{1}{N}\sum_i |C_i - C_i^{\text{exact}}| \tag{12.26}$$

L_2 norm (RMS error):

$$\|e\|_2 = \sqrt{\frac{1}{N}\sum_i (C_i - C_i^{\text{exact}})^2} \tag{12.27}$$

L_∞ norm (max error):

$$\|e\|_\infty = \max_i |C_i - C_i^{\text{exact}}| \tag{12.28}$$

12.8.2 Relative Error

$$e_{\text{rel}} = \frac{\|C - C^{\text{exact}}\|}{\|C^{\text{exact}}\|} \tag{12.29}$$

12.9 Uncertainty Quantification

12.9.1 Sources of Uncertainty

- **Aleatory**: Inherent randomness (stochastic processes)
- **Epistemic**: Lack of knowledge (uncertain parameters)
- **Numerical**: Discretization, round-off errors

12.9.2 Sensitivity Analysis

One-at-a-time:

$$S_i = \frac{\partial Q}{\partial p_i} \tag{12.30}$$

Variance-based (Sobol indices):

$$S_i = \frac{V[\mathbb{E}[Q|p_i]]}{V[Q]} \tag{12.31}$$

12.9.3 Parameter Estimation

Bayesian inference:

$$P(\theta|D) \propto P(D|\theta)P(\theta) \tag{12.32}$$

Methods:

- Markov Chain Monte Carlo (MCMC)
- Approximate Bayesian Computation (ABC)
- Ensemble Kalman Filter

12.10 Best Practices

12.10.1 Code Development

1. Write unit tests for all functions
2. Use version control (git)
3. Document assumptions and limitations
4. Continuous integration testing

12.10.2 Simulation Workflow

1. Verify code with MMS
2. Run benchmark problems
3. Perform convergence study
4. Quantify uncertainty
5. Compare to experiments (validation)
6. Document all parameters and settings

12.10.3 Reproducibility

- Save all input files
- Record software versions
- Use deterministic random seeds
- Archive raw output data

12.11 Mesoscale-Specific Challenges

12.11.1 Multi-Scale Verification

Each component must be verified:

- Fluid solver alone
- Diffusion solver alone
- Agent mechanics alone
- Coupling operators
- Full coupled system

12.11.2 Stochastic Validation

Agent-based models are stochastic:

- Run ensemble of simulations
- Compare distributions, not single realizations
- Use statistical tests (Kolmogorov-Smirnov, etc.)

12.11.3 Emergent Properties

Validate emergent behavior:

- Pattern formation
- Collective migration
- Growth kinetics
- Morphology statistics

12.12 Summary

Key Concepts

- **Time integration**: Explicit (conditional stability) vs. implicit (unconditional)
- **Spatial discretization**: CFL condition limits explicit advection/diffusion
- **Verification**: Code solves equations correctly (MMS, benchmarks)
- **Validation**: Model represents reality (experimental comparison)

- **Convergence studies**: Verify order of accuracy with grid/time refinement
- **Uncertainty quantification**: Essential for predictive simulations

12.13 Further Reading

1. Roache, P.J. (1998). *Verification and Validation in Computational Science and Engineering*. Hermosa.

2. LeVeque, R.J. (2007). *Finite Difference Methods for Ordinary and Partial Differential Equations*. SIAM.

3. Oberkampf, W.L. & Roy, C.J. (2010). *Verification and Validation in Scientific Computing*. Cambridge.

4. Smith, R.C. (2014). *Uncertainty Quantification*. SIAM.

Part IV

Application Case Studies

Chapter 13

Gastrointestinal Dynamics

13.1 Introduction

The gastrointestinal (GI) tract is a paradigmatic mesoscale system:

- Complex geometry (villi, crypts, folds)
- Multi-physics (flow, transport, mechanics, biology)
- Active motility (peristalsis, segmentation)
- Host-microbiome interactions

13.2 Anatomy at the Mesoscale

13.2.1 Intestinal Wall Structure

From lumen to serosa:

1. **Mucosa**: Epithelium + lamina propria + muscularis mucosae
2. **Submucosa**: Connective tissue + blood/lymph vessels + nerves
3. **Muscularis externa**: Circular + longitudinal smooth muscle
4. **Serosa**: Connective tissue covering

13.2.2 Villus Architecture

Small intestinal villi:

Property	**Value**
Height	0.5–1.5 mm
Diameter	0.1–0.2 mm
Density	10–40 villi/mm^2
Surface amplification	6–10 ×

Each villus contains:

- Central lacteal (lymphatic)
- Capillary network
- Smooth muscle core (allows contraction)
- Epithelial monolayer with enterocytes

13.2.3 Crypts of Lieberkühn

Intestinal stem cell niche:

- Depth: 250–500 μm
- Contain stem cells at base
- Site of cell proliferation
- Cells migrate up to villus tip
- Transit time: 3–5 days

13.3 Fluid Dynamics

13.3.1 Luminal Flow

Chyme (partially digested food) properties:

Property	Range
Viscosity	1–100 mPa·s (shear-thinning)
Density	1000–1100 kg/m^3
Flow rate	1–10 mL/min
Reynolds number	0.01–10

13.3.2 The Unstirred Water Layer

Adjacent to the epithelium:

- Thickness: 100–400 μm (measured by various techniques)
- Creates diffusion barrier
- Affects nutrient absorption rates
- Reduced by villus motility and luminal mixing

Effective permeability:

$$P_{\text{eff}} = \frac{1}{1/P_{\text{UWL}} + 1/P_{\text{membrane}}} \tag{13.1}$$

where $P_{\text{UWL}} = D/\delta$ (diffusion coefficient / layer thickness).

13.3.3 Villus Tip Flow

Near villus tips:

- Flow velocities: 10–100 μm/s
- Local Re ~ 0.01
- Stokes flow regime
- Enhanced mixing from villus motion

13.4 Motility Patterns

13.4.1 Peristalsis

Coordinated muscle contraction waves:

- Frequency: 10–12 contractions/min (small intestine)
- Wave speed: 1–2 cm/s
- Propels contents aborally

Mathematical model:

$$R(z,t) = R_0 - a\cos\left(\frac{2\pi}{\lambda}(z-ct)\right) \tag{13.2}$$

where R_0 is mean radius, a is amplitude, λ is wavelength, c is wave speed.

13.4.2 Segmentation

Localized contractions without net propulsion:

- Mixes luminal contents
- Enhances nutrient contact with mucosa
- Alternating contraction-relaxation pattern

13.4.3 Villus Motility

Individual villi contract rhythmically:

- Frequency: 6–12 contractions/min
- Shortening: 10–30% of length
- Driven by muscularis mucosae
- Enhances lymphatic pumping
- Reduces effective UWL thickness

13.5 Mass Transport

13.5.1 Nutrient Absorption

Key nutrients and mechanisms:

Nutrient	**Mechanism**	**Location**
Glucose	SGLT1 (active), GLUT2	Duodenum, jejunum
Amino acids	Various transporters	Jejunum
Fatty acids	Passive diffusion	Jejunum
Vitamin B12	Intrinsic factor	Terminal ileum
Bile salts	Active transport	Terminal ileum
Water	Osmosis	Throughout

13.5.2 Transport Equations

Advection-diffusion with uptake:

$$\frac{\partial C}{\partial t} + \mathbf{u} \cdot \boldsymbol{\nabla} C = D\nabla^2 C - k_{\text{uptake}} C \cdot \delta_{\text{surface}} \tag{13.3}$$

For Michaelis-Menten uptake:

$$J_{\text{uptake}} = \frac{V_{\max} C}{K_m + C} \tag{13.4}$$

13.5.3 Peclet Number Effects

Solute	D **[m^2/s]**	**Pe**
Glucose	6×10^{-10}	100–1000
Amino acid	5×10^{-10}	100–1000
Bile salt micelle	1×10^{-10}	500–5000
Fatty acid	5×10^{-10}	100–1000

High Pe implies advection-dominated transport with boundary layer effects.

13.6 Gas Transport and Bubbles

13.6.1 Sources of Intestinal Gas

- Swallowed air (N_2, O_2)
- Bacterial fermentation (H_2, CO_2, CH_4)
- Diffusion from blood (CO_2)
- Chemical reactions (CO_2 from bicarbonate)

13.6.2 Gas Composition

Gas	**Fraction**
N_2	20–90%
H_2	0–50%
CO_2	5–50%
CH_4	0–30%
O_2	0–10%

13.6.3 Bubble Dynamics

Bubble behavior governed by:

$$\frac{dR}{dt} = \frac{D}{R}\left(\frac{C_\infty - C_R}{C_R}\right) \tag{13.5}$$

where C_R is the gas concentration at the bubble surface (Henry's law).
Small bubbles dissolve; large bubbles grow and coalesce.

13.6.4 Gas Trapping

Pathological gas retention:

- Mechanical obstruction
- Dysmotility
- Excessive production
- Reduced absorption

13.7 Microbiome Interactions

13.7.1 Spatial Distribution

Region	Bacterial Load [CFU/mL]
Stomach	10^1–10^3
Duodenum	10^3–10^4
Jejunum	10^4–10^5
Ileum	10^7–10^8
Colon	10^{11}–10^{12}

13.7.2 Bacterial Metabolism

Key metabolic processes:

- Fermentation: carbohydrates → short-chain fatty acids (SCFA)
- Bile salt metabolism
- Vitamin synthesis (K, B12, folate)
- Gas production

13.7.3 Mucus Layer

Barrier between bacteria and epithelium:

- Thickness: 100–800 μm (colon: dual layer)
- Inner layer: dense, sterile
- Outer layer: loose, colonized
- Turnover: 1–2 hours

13.8 Pathophysiology

13.8.1 Infant Colic

Characteristics:

- Rule of 3s: >3 hours crying, >3 days/week, >3 weeks
- Affects 10–30% of infants

- Peak at 6 weeks, resolves by 3–4 months

Proposed mesoscale mechanisms:

- Immature motility patterns
- Gas bubble trapping
- Visceral hypersensitivity
- Gut-brain axis dysregulation

13.8.2 Necrotizing Enterocolitis (NEC)

Devastating neonatal disease:

- Primarily affects premature infants
- Mortality: 20–30%
- Involves intestinal necrosis

Mesoscale factors:

- Immature barrier function
- Abnormal microbial colonization
- Hypoxic-ischemic injury
- Dysregulated inflammatory response
- Gas (pneumatosis intestinalis)

13.8.3 Inflammatory Bowel Disease

Crohn's disease and ulcerative colitis:

- Altered mucus layer
- Bacterial translocation
- Immune dysregulation
- Motility changes

13.9 Computational Modeling

13.9.1 Geometry Generation

Villus array representation:

```
def generate_villus_field(nx, ny, villus_params):
    """Generate 2D villus geometry field."""
    field = np.zeros((nx, ny))
    for i, (x, y) in enumerate(villus_positions):
        field += villus_shape(x, y, villus_params[i])
    return field
```

13.9.2 LBM for Intestinal Flow

Peristaltic flow with moving boundaries:

- IBM for wall motion
- Non-Newtonian viscosity for chyme
- Coupled advection-diffusion for nutrients

13.9.3 Agent-Based Epithelium

Epithelial cell dynamics:

- Stem cells in crypt base
- Transit-amplifying cells
- Differentiation along crypt-villus axis
- Shedding at villus tip

13.10 Experimental Validation

13.10.1 In Vitro Models

Gut-on-chip platforms:

- Caco-2 cell monolayers
- 3D organoid cultures
- Peristaltic strain (10% at 0.15 Hz)
- Flow (shear stress 0.02 dyne/cm^2)

13.10.2 In Vivo Imaging

- Capsule endoscopy
- MRI for motility
- Contrast-enhanced CT
- Fluorescence imaging (animal models)

13.10.3 Key Measurements

Parameter	**Method**
Transit time	Radiopaque markers
Motility index	Manometry
Absorption rate	Tracer studies
Barrier function	TEER, permeability markers
Microbiome	16S sequencing

13.11 The Prize: Clinical Applications

13.11.1 Drug Delivery

Understanding mesoscale transport enables:

- Optimized oral drug formulations
- Targeted release strategies
- Prediction of bioavailability

13.11.2 Nutritional Interventions

- Optimized infant formula design
- Prebiotic/probiotic delivery
- Malabsorption treatment

13.11.3 Disease Treatment

- Physical interventions for gas management
- Motility-targeting therapies
- Barrier-enhancing strategies

13.12 Summary

Key Concepts

- **Villus architecture** amplifies surface area 6–10×
- **Unstirred water layer** (100–400 μm) limits absorption
- **Peristalsis and villus motility** enhance mixing and transport
- **High Peclet numbers** indicate advection-dominated transport
- **Gas dynamics** involve production, absorption, and bubble behavior
- **Infant colic and NEC** may involve mesoscale transport dysfunction

13.13 Further Reading

1. Lentle, R.G. & Janssen, P.W.M. (2011). *The Physical Processes of Digestion*. Springer.
2. Fung, Y.C. (1993). *Biomechanics: Mechanical Properties of Living Tissues*, Ch. 11. Springer.
3. Kim, H.J. et al. (2012). "Human gut-on-a-chip inhabited by microbial flora." *Lab Chip*.
4. Caplan, M.S. & Jilling, T. (2001). "New concepts in necrotizing enterocolitis." *Current Opinion in Pediatrics*.

Chapter 14

The Glymphatic System

14.1 Introduction

The glymphatic system is a recently discovered (2012) brain waste clearance pathway:

- Clears metabolic waste from the brain
- Uses perivascular spaces for bulk flow
- Enhanced during sleep
- Dysfunction implicated in neurodegenerative disease

The name "glymphatic" reflects the role of glial cells (astrocytes) in a lymphatic-like function.

14.2 Anatomy of the Glymphatic System

14.2.1 Perivascular Spaces

Fluid channels surrounding blood vessels:

Location	**Structure**	**Width**
Pial surface	Virchow-Robin spaces	10–100 μm
Penetrating arteries	Peri-arterial	20–50 μm
Capillaries	Basement membrane	$\sim$20 nm
Veins	Peri-venous	20–50 μm

14.2.2 Astrocyte Endfeet

Astrocyte processes form the outer boundary:

- Dense coverage of penetrating vessels
- AQP4 water channels concentrated here
- Form part of blood-brain barrier
- "Polarization": AQP4 at endfeet $>$ soma

14.2.3 Aquaporin-4 (AQP4)

Water channel protein critical for glymphatic function:

- Tetrameric membrane protein
- Highly water-selective
- Enables rapid water flux
- Knockout mice show impaired clearance

14.3 The Glymphatic Pathway

14.3.1 Flow Route

1. CSF enters brain along peri-arterial spaces
2. Driven by arterial pulsations
3. Crosses into parenchyma (mechanism debated)
4. Mixes with interstitial fluid (ISF)
5. Exits along peri-venous spaces
6. Drains to meningeal lymphatics

14.3.2 Schematic

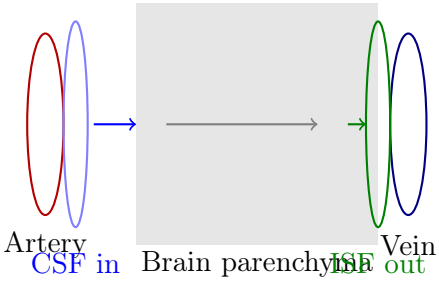

14.4 Driving Mechanisms

14.4.1 Arterial Pulsation

Primary driver of perivascular flow:

- Cardiac cycle: ∼1 Hz
- Wall displacement: 1–3% of diameter
- Creates pressure waves in PVS
- "Perivascular pumping"

Estimated effect:

$$u_{\text{PVS}} \propto \frac{\Delta R}{R} \cdot \omega \cdot R \tag{14.1}$$

14.4.2 Respiratory Pulsation

Secondary driver:

- Frequency: ∼0.2 Hz
- Affects intracranial pressure
- May modulate flow direction

14.4.3 Vasomotion

Spontaneous smooth muscle contractions:

- Frequency: 0.01–0.1 Hz
- Amplitude: 5–20% diameter change
- Traveling waves along vessels
- May significantly contribute to flow

14.4.4 Relative Contributions

Based on computational modeling and experiments:

Mechanism	Estimated Contribution
Cardiac pulsation	40–60%
Vasomotion	20–40%
Respiration	10–20%
Diffusion alone	Insufficient

14.5 Transport Physics

14.5.1 Characteristic Numbers

Number	Formula	PVS Value
Reynolds	$\mathrm{Re} = UL/\nu$	0.001–0.1
Womersley	$\mathrm{Wo} = R\sqrt{\omega/\nu}$	0.1–0.5
Peclet	$\mathrm{Pe} = UL/D$	10–1000

Low Re implies Stokes flow; low Wo implies quasi-steady response.

14.5.2 Perivascular Space Flow

For annular geometry with pulsating inner wall:

$$\frac{\partial p}{\partial z} = \mu \left(\frac{1}{r} \frac{\partial}{\partial r} \left(r \frac{\partial u}{\partial r} \right) \right) \tag{14.2}$$

With oscillating inner boundary $R_i(t) = R_{i0}(1 + \epsilon \cos(\omega t))$.

14.5.3 Dispersion Enhancement

Even without net flow, pulsation enhances transport:

$$D_{\text{eff}} = D + \frac{U^2 T}{48\pi^2 D} \cdot f(\text{geometry}) \tag{14.3}$$

Taylor-Aris dispersion in oscillatory flow.

14.6 Solute Clearance

14.6.1 Key Solutes

Solute	**MW [kDa]**	D **[m^2/s]**	**Clearance**
Lactate	0.09	10^{-9}	Fast
Glucose	0.18	6×10^{-10}	Fast
Aβ_{1-40}	4.3	1.5×10^{-10}	Hours
Aβ_{1-42}	4.5	1.4×10^{-10}	Hours
Tau	45	4×10^{-11}	Slow
α-synuclein	14	8×10^{-11}	Slow

14.6.2 Clearance Rate Model

First-order clearance:

$$\frac{d[\text{A}\beta]}{dt} = P - k_{\text{clear}}[\text{A}\beta] \tag{14.4}$$

where P is production rate and k_{clear} depends on glymphatic efficiency.
Half-life:

$$t_{1/2} = \frac{\ln 2}{k_{\text{clear}}} \tag{14.5}$$

Typical Aβ half-life: 6–12 hours.

14.7 Sleep-Wake Modulation

14.7.1 The Sleep Discovery

Xie et al. (2013) showed 60% increase in ISF space during sleep:

- Anesthetized mice: similar to natural sleep
- Awake mice: reduced ISF volume
- Tracer clearance 2× faster in sleep

14.7.2 Mechanisms

1. **Norepinephrine decrease**: Astrocyte shrinkage increases ISF space
2. **Brain state**: Slow-wave activity may enhance flow
3. **Posture**: Lateral position may optimize drainage
4. **Cardiovascular changes**: Blood pressure, heart rate patterns

14.7.3 Quantitative Changes

Parameter	Wake	Sleep
ISF volume fraction	14%	23%
Aβ clearance rate	k_w	$2k_w$
Tortuosity	Higher	Lower
AQP4 polarization	Normal	Enhanced

14.8 Implications for Neurodegenerative Disease

14.8.1 Alzheimer's Disease

Aβ accumulation may result from clearance failure:

- Age-related reduction in glymphatic function
- AQP4 depolarization with age
- Arterial stiffening reduces pulsatility
- Sleep disturbance compounds problem

Vicious cycle:

$$\text{A}\beta \uparrow \rightarrow \text{Sleep disruption} \rightarrow \text{Clearance} \downarrow \rightarrow \text{A}\beta \uparrow \tag{14.6}$$

14.8.2 Parkinson's Disease

α-synuclein clearance:

- Aggregates in Lewy bodies
- May spread via glymphatic pathway
- Sleep disorders common in PD

14.8.3 Traumatic Brain Injury

Post-TBI changes:

- Acute: enhanced clearance (good)
- Chronic: impaired function
- May explain delayed neurodegeneration

14.9 Computational Modeling

14.9.1 Geometry

Perivascular space models:

- Annular (concentric cylinders)
- Eccentric (realistic positioning)
- Elliptical cross-sections
- Branching networks

14.9.2 LBM Implementation

From Chapter 9, LBM is well-suited for PVS flow:

```
# Pulsatile wall velocity boundary condition
def wall_velocity(t, amplitude, frequency):
    return amplitude * np.sin(2 * np.pi * frequency * t)

# Run LBM with IBM for wall motion
for step in range(n_steps):
    t = step * dt
    solver.set_inner_wall_velocity(wall_velocity(t, A, f))
    solver.step()
```

14.9.3 Coupled Transport

Advection-diffusion for solute:

$$\frac{\partial C}{\partial t} + \mathbf{u} \cdot \boldsymbol{\nabla} C = D \nabla^2 C \tag{14.7}$$

with $\mathbf{u}$ from LBM solution.

14.9.4 Network Models

For whole-brain scale:

- Reduced 1D models along vessels
- Graph-based network representation
- Coupled ODEs for compartments

14.10 Experimental Techniques

14.10.1 In Vivo Imaging

Technique	Resolution	Information
Two-photon microscopy	0.5 μm	PVS geometry, tracer dynamics
MRI (phase contrast)	100 μm	Bulk CSF flow
Contrast-enhanced MRI	0.5 mm	Tracer distribution
PET	1 mm	Metabolite clearance

14.10.2 Tracer Studies

Common tracers:

- Fluorescent dextrans (various MW)
- Ovalbumin (45 kDa)
- Quantum dots
- Gadolinium (MRI)

14.10.3 Key Experiments

1. Iliff et al. (2012): Identified paravascular pathway
2. Xie et al. (2013): Sleep enhancement of clearance
3. Mestre et al. (2018): Arterial pulsation drives flow
4. Nedergaard lab: AQP4 knockout studies

14.11 Current Debates

14.11.1 Bulk Flow vs. Dispersion

Controversy over transport mechanism:

- **Bulk flow proponents**: Net directional CSF flow through parenchyma
- **Dispersion proponents**: Oscillatory flow + enhanced diffusion
- Reality: likely combination, varies by location

14.11.2 Parenchymal Transport

How does fluid/solute traverse brain tissue?

- Through ISF channels?
- Along white matter tracts?
- Cell-to-cell transport?

Brain permeability: $K \sim 10^{-17}$–10^{-15} m^2 (very low).

14.12 Therapeutic Opportunities

14.12.1 Sleep Optimization

Enhancing natural clearance:

- Sleep quality interventions
- Body position during sleep
- Treatment of sleep disorders

14.12.2 Physical Enhancement

External driving:

- Low-intensity focused ultrasound
- Transcranial vibration
- Exercise effects

14.12.3 Pharmacological Targets

- AQP4 modulators
- Vasomotion enhancers
- Norepinephrine pathway

14.13 The Prize

Better understanding of glymphatic flow could:

1. Enable early detection of clearance impairment
2. Guide preventive interventions (sleep, exercise)
3. Identify drug targets for neurodegeneration
4. Optimize timing of therapies (sleep-wake cycle)
5. Improve drug delivery to CNS

Potential impact: 6+ million Alzheimer's patients in US alone.

14.14 Summary

Key Concepts

- **Glymphatic system**: Brain waste clearance via perivascular spaces
- **Arterial pulsation**: Primary driver of PVS flow
- **AQP4 polarization**: Critical for water flux at astrocyte endfeet
- **Sleep enhancement**: 2× increased clearance during sleep
- **Neurodegeneration**: Impaired clearance linked to Aβ accumulation
- **Low Reynolds number**: Stokes flow regime in PVS

14.15 Further Reading

1. Iliff, J.J. et al. (2012). "A paravascular pathway facilitates CSF flow through the brain parenchyma." *Science Translational Medicine*.
2. Xie, L. et al. (2013). "Sleep drives metabolite clearance from the adult brain." *Science*.
3. Mestre, H. et al. (2018). "Flow of cerebrospinal fluid is driven by arterial pulsations." *Nature Communications*.
4. Nedergaard, M. & Goldman, S.A. (2020). "Glymphatic failure as a final common pathway to dementia." *Science*.

Chapter 15

Vascular Networks and Oxygen Delivery

15.1 Introduction

The vascular system is the quintessential mesoscale transport network:

- Delivers oxygen and nutrients to every cell
- Removes metabolic waste
- Spans scales from aorta (25 mm) to capillaries (5 μm)
- Exhibits optimal branching architecture

15.2 Vascular Architecture

15.2.1 Hierarchy of Vessels

Vessel Type	**Diameter**	**Wall Thickness**	**Function**
Aorta	25 mm	2 mm	Elastic reservoir
Large artery	4–10 mm	1 mm	Conduit
Small artery	0.5–4 mm	0.5 mm	Conduit
Arteriole	10–100 μm	6–20 μm	Resistance
Capillary	5–10 μm	0.5 μm	Exchange
Venule	10–100 μm	2–5 μm	Collection
Vein	0.5–5 mm	0.5 mm	Capacitance

15.2.2 Capillary Density

Varies by tissue metabolic demand:

Tissue	**Capillary Density [cap/mm^2]**
Skeletal muscle (resting)	200–400
Skeletal muscle (active)	400–800
Heart muscle	2500–4000
Brain gray matter	1000–1500
Brain white matter	400–600
Liver	1000–1500

15.2.3 Total Network Statistics

Human body:

- Total capillary length: ∼60,000 km
- Total capillary surface area: ∼300 m^2
- Blood volume in capillaries: ∼250 mL (5% of total)
- Transit time through capillary: 0.5–2 s

15.3 Murray's Law Revisited

15.3.1 Derivation (from Chapter 4)

Optimal branching minimizes total power:

$$W = W_{\text{pump}} + W_{\text{metabolic}} = \frac{8\mu L Q^2}{\pi r^4} + b\pi r^2 L \tag{15.1}$$

Result:

$$\boxed{r_0^3 = r_1^3 + r_2^3} \tag{15.2}$$

15.3.2 Experimental Validation

Murray's law holds approximately:

Vascular Bed	Measured Exponent	Theory
Aorta-iliac	2.7–2.9	3.0
Coronary arteries	2.5–2.8	3.0
Mesenteric	2.8–3.0	3.0
Retinal	2.6–2.8	3.0

Deviations may indicate pathology.

15.3.3 Implications for Shear Stress

If Murray's law holds:

$$\tau_w = \frac{4\mu Q}{\pi r^3} = \text{constant throughout network} \tag{15.3}$$

Typical value: 15–20 dyne/cm^2 in healthy arteries.

15.4 Blood Flow Dynamics

15.4.1 Pulsatile Flow

In larger vessels, flow is unsteady:

$$Q(t) = Q_0 + \sum_{n=1}^{N} Q_n \cos(n\omega t + \phi_n) \tag{15.4}$$

Womersley solution describes velocity profile (Chapter 5).

15.4.2 Microcirculatory Flow

In capillaries:

- Reynolds number: $\text{Re} \sim 10^{-2}$
- Single-file RBC passage
- Plasma skimming at bifurcations
- Non-continuum effects

15.4.3 Phase Separation

At bifurcations, hematocrit differs between branches:

$$\frac{H_1}{H_0} \neq \frac{Q_1}{Q_0} \tag{15.5}$$

The smaller branch receives proportionally less RBCs (plasma skimming).

15.5 Oxygen Transport

15.5.1 Oxygen Cascade

Partial pressures decrease from atmosphere to mitochondria:

Location	$P_{\mathbf{O_2}}$ **[mmHg]**
Atmosphere	160
Alveolar gas	100
Arterial blood	95
Tissue average	20–40
Venous blood	40
Mitochondria	1–5

15.5.2 Hemoglobin Binding

Oxygen-hemoglobin dissociation curve (Hill equation):

$$S_{\text{O}_2} = \frac{P_{\text{O}_2}^n}{P_{50}^n + P_{\text{O}_2}^n} \tag{15.6}$$

with $n \approx 2.7$ and $P_{50} \approx 26$ mmHg.
Bohr effect (pH dependence) and 2,3-DPG shift the curve.

15.5.3 Oxygen Content

Total oxygen in blood:

$$C_{\text{O}_2} = 1.34 \cdot [\text{Hb}] \cdot S_{\text{O}_2} + 0.003 \cdot P_{\text{O}_2} \tag{15.7}$$

where [Hb] is hemoglobin concentration (g/dL).

15.5.4 Krogh Cylinder Model

Classical tissue oxygen model (Chapter 6):

$$D_{O_2}\left(\frac{1}{r}\frac{d}{dr}\left(r\frac{dP_{O_2}}{dr}\right)\right) = M_0 \tag{15.8}$$

Solution:

$$P_{O_2}(r) = P_c - \frac{M_0}{4D_{O_2}}(r^2 - R_c^2) - \frac{M_0 R_t^2}{2D_{O_2}}\ln\left(\frac{r}{R_c}\right) \tag{15.9}$$

15.5.5 Critical Tissue Radius

Maximum radius that can be supplied:

$$R_t^{\text{crit}} = \sqrt{\frac{4\alpha D_{O_2} P_c}{M_0}} \tag{15.10}$$

Typical values: 100–200 μm, explaining capillary spacing.

15.6 Liver Lobule Perfusion

15.6.1 Lobule Architecture

The liver is organized into hexagonal lobules:

- Diameter: 1–2 mm
- Central vein at center
- Portal triads at corners (hepatic artery, portal vein, bile duct)
- Blood flows centripetally

15.6.2 Metabolic Zonation

Oxygen gradient creates functional zones:

Zone	**Location**	P_{O_2}	**Function**
Zone 1	Periportal	60–70 mmHg	Gluconeogenesis, β-oxidation
Zone 2	Mid-lobule	35–50 mmHg	Mixed metabolism
Zone 3	Pericentral	25–35 mmHg	Glycolysis, lipogenesis, drug metabolism

15.6.3 Modeling Considerations

- Dual blood supply (75% portal vein, 25% hepatic artery)
- Sinusoidal flow (very low Re)
- Fenestrated endothelium
- Hepatocyte oxygen consumption

15.7 Angiogenesis

15.7.1 Process

New vessel formation from existing vessels:

1. Hypoxia induces HIF-1α
2. VEGF secretion
3. Endothelial tip cell selection
4. Sprout extension and branching
5. Lumen formation
6. Perfusion and remodeling

15.7.2 Computational Models

Agent-based endothelial cells:

```
class TipCell(Agent):
    def migrate(self, vegf_field):
        # Chemotaxis up VEGF gradient
        gradient = compute_gradient(vegf_field, self.position)
        self.velocity = chi * gradient / |gradient|
        self.position += self.velocity * dt

    def branch(self, probability):
        if random() < probability * dt:
            spawn_new_tip_cell()
```

15.7.3 Network Remodeling

After initial sprouting:

- Anastomosis (connection of sprouts)
- Flow initiation
- Pruning of non-perfused vessels
- Diameter adaptation to flow

Adaptation rule:

$$\frac{dR}{dt} = k(\tau_w - \tau_{\text{set}})R \tag{15.11}$$

Vessels adjust to maintain target shear stress.

15.8 Tumor Vasculature

15.8.1 Characteristics

Tumor vessels are highly abnormal:

- Tortuous, dilated, irregular

- Leaky (fenestrations, gaps)
- Poor pericyte coverage
- Abnormal branching (violate Murray's law)
- Intermittent flow

15.8.2 Consequences

- Heterogeneous oxygenation (hypoxic regions)
- High interstitial pressure
- Poor drug delivery
- Therapeutic resistance

15.8.3 Vascular Normalization

Anti-VEGF therapy can "normalize" vessels:

- Prune excess vessels
- Reduce leakiness
- Improve perfusion temporarily
- Enhance chemotherapy window

15.9 Computational Network Models

15.9.1 Graph Representation

Vascular network as graph:

- Nodes: bifurcations, endpoints
- Edges: vessel segments
- Edge properties: length, diameter, flow

15.9.2 Flow Solution

Kirchhoff's laws:

$$\sum_j Q_{ij} = 0 \quad \text{(mass conservation)} \tag{15.12}$$

$$Q_{ij} = G_{ij}(P_i - P_j) \quad \text{(Poiseuille)} \tag{15.13}$$

where $G_{ij} = \pi R_{ij}^4/(8\mu L_{ij})$ is the conductance.
Results in linear system for pressures.

15.9.3 Oxygen Transport in Networks

Coupled blood-tissue transport:

$$\frac{d(Q \cdot C_{O_2})}{ds} = -j_{\text{wall}}(s) \tag{15.14}$$

where j_{wall} is the flux to tissue.

15.9.4 Green's Function Methods

For tissue oxygen field:

$$P_{O_2}(\mathbf{x}) = \sum_i \int_{\text{vessel } i} G(\mathbf{x}, \mathbf{x}') j(s') ds' \tag{15.15}$$

where G is the Green's function for the diffusion equation.

15.10 Experimental Techniques

15.10.1 Network Imaging

Technique	Resolution	Scale
Confocal microscopy	0.5 μm	mm
Two-photon microscopy	0.5 μm	mm (deeper)
Micro-CT (contrast)	5–20 μm	cm
Light-sheet microscopy	1 μm	mm
OCT angiography	5 μm	mm

15.10.2 Flow Measurements

- Particle tracking velocimetry
- Laser Doppler flowmetry
- RBC velocity from line scans
- MRI phase contrast

15.10.3 Oxygen Measurements

- Phosphorescence quenching
- Two-photon P_{O_2} probes
- Electrode measurements
- BOLD fMRI (indirect)

15.11 Clinical Relevance

15.11.1 Atherosclerosis

Plaque forms at low/oscillatory shear stress regions:

- Bifurcations, inner curvatures
- Deviation from Murray's law
- Altered hemodynamics

15.11.2 Diabetic Retinopathy

- Abnormal angiogenesis
- Capillary dropout
- Vision loss

15.11.3 Peripheral Vascular Disease

- Reduced blood flow to extremities
- Tissue hypoxia
- Poor wound healing

15.12 The Prize

Understanding vascular networks enables:

1. Optimized drug delivery strategies
2. Early detection of vascular dysfunction
3. Tissue engineering with proper vascularization
4. Anti-angiogenic therapy optimization
5. Personalized cardiovascular risk assessment

15.13 Summary

Key Concepts

- **Murray's Law** optimizes vascular branching ($r_0^3 = r_1^3 + r_2^3$)
- **Krogh cylinder** model describes tissue oxygenation
- **Capillary spacing** ($\sim$100–200 μm) set by diffusion limits
- **Metabolic zonation** in liver reflects oxygen gradients
- **Angiogenesis** is VEGF-driven with tip cell chemotaxis
- **Tumor vessels** violate normal architecture; can be normalized

15.14 Further Reading

1. Pries, A.R. et al. (2005). "The microcirculation: Physiology at the mesoscale." *Journal of Physiology.*
2. Secomb, T.W. (2017). "Blood flow in the microcirculation." *Annual Review of Fluid Mechanics.*
3. Carmeliet, P. & Jain, R.K. (2011). "Principles and mechanisms of vessel normalization." *Nature Reviews Drug Discovery.*
4. Goldman, D. (2008). "Theoretical models of microvascular oxygen transport." *Microcirculation.*

Part V

Experimental Techniques and Future Directions

Chapter 16

Organ-on-Chip Platforms

16.1 Introduction

Organ-on-chip (OoC) devices are microengineered systems that:

- Recapitulate key aspects of organ physiology
- Provide controlled mechanical and chemical environments
- Enable real-time observation
- Bridge the gap between cell culture and animal models

16.2 Design Principles

16.2.1 Key Requirements

Effective organ chips must provide:

1. **Relevant cell types**: Primary or iPSC-derived
2. **Tissue architecture**: 3D organization, interfaces
3. **Mechanical forces**: Flow, strain, pressure
4. **Biochemical gradients**: Oxygen, nutrients, signals
5. **Measurement access**: Imaging, sampling, sensors

16.2.2 Microfluidic Fundamentals

Flow in microchannels:

$$\text{Re} = \frac{\rho U D_h}{\mu} \sim 0.01\text{–}10 \tag{16.1}$$

where D_h is the hydraulic diameter.
At these scales:

- Laminar flow (no turbulence)
- Predictable concentration gradients
- Surface effects dominate

16.2.3 Shear Stress Control

Wall shear stress in rectangular channel:

$$\tau_w = \frac{6\mu Q}{wh^2} \tag{16.2}$$

where w is width and h is height.
Physiological ranges:

Tissue	Shear Stress [dyne/cm^2]
Endothelium (arterial)	10–70
Endothelium (venous)	1–6
Intestinal epithelium	0.02–0.08
Renal tubule	0.1–1

16.3 Gut-on-Chip

16.3.1 Design Features

The Wyss Institute gut chip:

- Two channels separated by porous membrane
- Upper: epithelial cells (Caco-2 or organoid-derived)
- Lower: endothelial cells
- Cyclic strain (10% at 0.15 Hz) mimics peristalsis
- Flow creates physiological shear

16.3.2 Key Parameters

Parameter	Value
Channel dimensions	1 mm × 0.2 mm × 20 mm
Flow rate	30–60 μL/h
Shear stress	0.02 dyne/cm^2
Strain	10% at 0.15 Hz
Membrane pore size	10 μm

16.3.3 Biological Outcomes

With mechanical stimulation:

- Spontaneous villus-like folding
- Improved barrier function (higher TEER)
- Mucus production
- Support of microbiome
- Differentiation of multiple cell types

16.3.4 Applications

- Drug absorption studies
- Microbiome-host interactions
- Inflammatory bowel disease models
- Food safety testing

16.4 Brain-on-Chip for Glymphatic Studies

16.4.1 Challenges

Modeling glymphatic function requires:

- Perivascular space geometry
- Astrocyte with AQP4 polarization
- Pulsatile boundary motion
- CSF flow and solute transport

16.4.2 Design Concepts

Peri-arterial chip:

- Central channel with pulsatile membrane
- Surrounding annular space (PVS mimic)
- Astrocyte-lined outer boundary
- Tracer injection and imaging

Brain slice perfusion:

- Organotypic brain slice
- Controlled artificial CSF flow
- Two-photon imaging of clearance

16.4.3 Key Parameters

Parameter	Target Value
PVS width	20–50 μm
Pulsation frequency	1 Hz (cardiac)
Wall displacement	1–3%
Flow velocity	10–100 μm/s
Tracer diffusivity	10^{-10}–10^{-9} m^2/s

16.5 Blood-Brain Barrier Chips

16.5.1 Architecture

Two-compartment design:

- Blood side: Brain endothelial cells + pericytes
- Brain side: Astrocytes + neurons (optional)
- Porous membrane between
- Flow on blood side

16.5.2 Validation Metrics

Metric	In Vivo	Chip Target
TEER	1500–2000 $\Omega \cdot cm^2$	>1000 $\Omega \cdot cm^2$
P_{app} (sucrose)	$< 10^{-7}$ cm/s	$< 10^{-6}$ cm/s
Efflux ratio	2–5	>2
Tight junctions	Continuous	Visualized

16.6 Lung-on-Chip

16.6.1 Design

Alveolar-capillary interface:

- Air-facing epithelial channel
- Blood-facing endothelial channel
- Thin membrane ($\sim$10 μm)
- Cyclic strain (5–15% at 0.2 Hz)

16.6.2 Applications

- Pulmonary edema modeling
- Drug-induced lung toxicity
- Infectious disease (influenza, SARS-CoV-2)
- Environmental toxin exposure

16.7 Heart-on-Chip

16.7.1 Design

Functional cardiac tissue:

- iPSC-derived cardiomyocytes
- Aligned tissue architecture
- Electrical stimulation
- Force measurement (pillars, cantilevers)

16.7.2 Key Readouts

- Beat rate and rhythm
- Contraction force
- Calcium transients
- Action potential duration
- Conduction velocity

16.8 Liver-on-Chip

16.8.1 Design Considerations

Recapitulating liver function:

- Hepatocyte zonation (oxygen gradient)
- Sinusoidal flow
- Bile canaliculi formation
- Non-parenchymal cells (Kupffer, stellate)

16.8.2 Oxygen Gradient Creation

Generate metabolic zonation:

$$\frac{dC_{O_2}}{dx} = -\frac{V_{max}}{Q} \cdot \frac{C_{O_2}}{K_m + C_{O_2}} \tag{16.3}$$

Creates periportal-to-pericentral gradient along channel.

16.9 Multi-Organ Systems

16.9.1 Body-on-Chip

Connecting multiple organs:

- Common circulation (blood substitute)
- Physiological flow ratios
- ADME studies (absorption, distribution, metabolism, excretion)

16.9.2 Scaling Laws

Allometric scaling for multi-organ:

$$\frac{V_{organ}}{V_{body}} = \text{constant} \tag{16.4}$$

Flow rates scale with organ size/function.

16.9.3 Challenges

- Common media compatibility
- Flow rate matching
- Residence time balance
- Bubble management
- Long-term stability

16.10 Fabrication Technologies

16.10.1 Soft Lithography

PDMS (polydimethylsiloxane) devices:

1. Design photomask
2. SU-8 master fabrication
3. PDMS casting
4. Plasma bonding

Advantages: Transparent, gas permeable, biocompatible, flexible. Limitations: Drug absorption, limited chemical resistance.

16.10.2 3D Printing

Direct fabrication:

- Stereolithography (SLA)
- Two-photon polymerization (high resolution)
- Digital light processing (DLP)

Resolution: 10–100 μm typical, down to 1 μm for two-photon.

16.10.3 Injection Molding

For scale-up:

- Thermoplastics (COC, PMMA, PS)
- High reproducibility
- Lower per-unit cost
- Less flexible for prototyping

16.11 Measurement Integration

16.11.1 Optical Access

Requirements for imaging:

- Optically clear materials
- Thin substrates for high-NA objectives
- Compatible with live-cell imaging

16.11.2 Integrated Sensors

Parameter	Sensor Type
Oxygen	Phosphorescent probes, Clark electrode
pH	ISFET, fluorescent dyes
TEER	Integrated electrodes
Flow rate	Thermal sensors, particle tracking
Strain	Embedded strain gauges

16.11.3 Sampling

- Effluent collection for metabolomics
- In-line sensors
- Microdialysis probes

16.12 Validation Strategies

16.12.1 Benchmark Comparisons

Compare to known in vivo data:

- Drug permeability coefficients
- Metabolic clearance rates
- Barrier function metrics
- Dose-response curves

16.12.2 Relevance vs. Convenience Trade-off

Model	Relevance	Convenience
Static 2D culture	Low	High
Transwell	Medium	Medium-High
Basic OoC	Medium-High	Medium
Complex OoC	High	Low
Organoid	High (structure)	Medium
Animal model	Variable	Low

16.13 Computational Modeling of OoC

16.13.1 Design Optimization

CFD to optimize:

- Channel geometry for uniform shear
- Bubble trap placement
- Gradient formation
- Oxygen delivery

16.13.2 Interpretation of Experiments

Modeling helps:

- Estimate shear stress distribution
- Calculate transport rates
- Predict concentration profiles
- Compare to physiological values

16.14 Regulatory Perspective

16.14.1 FDA Modernization Act 2.0

Recent legislation:

- Allows non-animal methods for drug approval
- OoC recognized as alternative
- Accelerating adoption

16.14.2 Qualification

Steps for regulatory acceptance:

1. Context of use definition
2. Qualification study design
3. Performance benchmarking
4. Documentation and reproducibility

16.15 Summary

Key Concepts

- **Organ-on-chip** devices recapitulate tissue-level physiology
- **Mechanical forces** (flow, strain) are critical for proper function

- **Gut-on-chip** spontaneously forms villi under cyclic strain
- **Brain-on-chip** can model glymphatic flow and clearance
- **Multi-organ systems** enable ADME studies
- **Validation** requires comparison to in vivo benchmarks

16.16 Further Reading

1. Bhatia, S.N. & Ingber, D.E. (2014). "Microfluidic organs-on-chips." *Nature Biotechnology*.
2. Huh, D. et al. (2010). "Reconstituting organ-level lung functions on a chip." *Science*.
3. Kim, H.J. et al. (2012). "Human gut-on-a-chip inhabited by microbial flora." *Lab on a Chip*.
4. Ingber, D.E. (2022). "Human organs-on-chips for disease modelling, drug development and personalized medicine." *Nature Reviews Genetics*.

Chapter 17

Imaging Techniques at the Mesoscale

17.1 Introduction

Mesoscale biology requires imaging techniques that can:

- Resolve cellular structures (∼1–10 μm)
- Cover tissue-scale fields of view (∼1–10 mm)
- Capture dynamic processes (ms–min time scales)
- Penetrate into intact tissue

17.2 Optical Microscopy Fundamentals

17.2.1 Resolution Limits

Abbe diffraction limit:

$$d = \frac{\lambda}{2 \cdot \mathrm{NA}} \tag{17.1}$$

Typical values:

Objective	NA	Resolution
10× air	0.3	1 μm
40× water	0.8	0.35 μm
63× oil	1.4	0.2 μm

17.2.2 Depth of Field

Axial resolution:

$$d_z = \frac{n\lambda}{\mathrm{NA}^2} \tag{17.2}$$

High NA gives better lateral resolution but shallower depth of field.

17.2.3 Light Scattering

In tissue, scattering limits penetration:

$$I(z) = I_0 e^{-\mu_s z} \tag{17.3}$$

Scattering coefficient $\mu_s \sim$ 10–100 mm^{-1} in tissue.

17.3 Confocal Microscopy

17.3.1 Principle

Point illumination + pinhole rejection of out-of-focus light:

- Optical sectioning capability
- Improved axial resolution
- Reduced background

17.3.2 Specifications

Parameter	Typical Value
Lateral resolution	0.2–0.5 μm
Axial resolution	0.5–1.5 μm
Penetration depth	50–200 μm
Acquisition speed	1–10 frames/s

17.3.3 Limitations

- Photobleaching from entire sample illumination
- Limited depth penetration
- Sequential scanning (slow for 3D)

17.4 Two-Photon Microscopy

17.4.1 Principle

Nonlinear excitation with near-infrared light:

$$\text{Fluorescence} \propto I^2 \tag{17.4}$$

Excitation only at focal point (intrinsic optical sectioning).

17.4.2 Advantages for Biology

- Deeper penetration (up to 1 mm)
- Less photobleaching (only focal volume excited)
- Less phototoxicity
- Better for live imaging

17.4.3 Specifications

Parameter	Typical Value
Excitation wavelength	700–1100 nm
Lateral resolution	0.3–0.5 μm
Axial resolution	1–2 μm
Penetration depth	500–1000 μm
Frame rate	1–30 Hz

17.4.4 Applications in Mesoscale Biology

- Glymphatic flow imaging (PVS tracer dynamics)
- Vascular network visualization
- Calcium imaging in intact tissue
- Cell migration in tumors

17.5 Light-Sheet Microscopy

17.5.1 Principle

Orthogonal illumination and detection:

- Thin sheet of light illuminates sample
- Camera captures entire plane at once
- Sample rotated/translated for 3D

17.5.2 Advantages

- Fast volumetric imaging
- Reduced photobleaching
- Large field of view
- Isotropic resolution possible (multi-view fusion)

17.5.3 Specifications

Parameter	Typical Value
Sheet thickness	1–10 μm
Field of view	mm–cm
Axial resolution	1–5 μm
Volume rate	0.1–10 Hz
Sample prep	Cleared or transparent

17.5.4 Tissue Clearing

Required for deep light-sheet imaging:

Method	Principle
CLARITY	Lipid removal, hydrogel embedding
iDISCO	Organic solvent dehydration
CUBIC	Aqueous clearing
uDISCO	Organic, preserves fluorescence

17.6 Particle Tracking Velocimetry

17.6.1 Principle

Track fluorescent particles to measure flow:

1. Seed flow with tracer particles
2. Image particle positions over time
3. Track individual particles or correlate patterns
4. Compute velocity field

17.6.2 Methods

PTV (Particle Tracking Velocimetry):

- Track individual particles
- Low seeding density
- Lagrangian velocities

PIV (Particle Image Velocimetry):

- Cross-correlate image patches
- Higher seeding density
- Eulerian velocity field

17.6.3 Specifications

Parameter	Range
Particle size	0.1–10 μm
Velocity range	1 μm/s – 10 m/s
Spatial resolution	10 μm – 1 mm
Temporal resolution	1 ms – 1 s

17.6.4 Applications

- Blood flow in microcirculation
- CSF flow in perivascular spaces
- Flow in organ-on-chip devices
- Intestinal lumen flow

17.7 Magnetic Resonance Imaging

17.7.1 Principle

Nuclear magnetic resonance of hydrogen nuclei:

- Magnetic field aligns spins
- RF pulses tip spins
- Relaxation produces signal
- Gradient fields encode spatial information

17.7.2 Phase-Contrast MRI

Velocity encoding via bipolar gradients:

$$\phi = \gamma \int_0^{TE} G(t) \cdot v \, dt \tag{17.5}$$

Velocity-to-phase relationship enables flow quantification.

17.7.3 Specifications for Flow Imaging

Parameter	**Typical Value**
Spatial resolution	0.5–2 mm
Temporal resolution	20–100 ms
Velocity range	0.1–100 cm/s
Penetration	Unlimited (non-invasive)

17.7.4 Applications

- CSF flow in ventricles and aqueduct
- Blood flow in major vessels
- Cardiac function
- Whole-brain glymphatic studies

17.7.5 Limitations

- Limited spatial resolution for mesoscale
- Cannot resolve individual cells
- Long acquisition times
- Motion artifacts

17.8 Ultrasound Imaging

17.8.1 Principle

Acoustic wave reflection:

- High-frequency sound waves (1–50 MHz)
- Reflection at tissue interfaces
- Doppler shift for motion detection

17.8.2 Doppler Ultrasound

Velocity from frequency shift:

$$\Delta f = \frac{2 f_0 v \cos\theta}{c} \tag{17.6}$$

17.8.3 Specifications

Parameter	Range
Frequency	1–50 MHz
Axial resolution	0.1–1 mm
Penetration	1–20 cm
Frame rate	10–1000 Hz

17.8.4 Functional Ultrasound

High-frame-rate ultrasound for brain imaging:

- Plane wave imaging
- Sensitive to small blood flow changes
- fUS: functional ultrasound imaging
- Spatial resolution: 100 μm

17.9 Optical Coherence Tomography

17.9.1 Principle

Low-coherence interferometry:

- Depth resolution from coherence gating
- Similar to ultrasound but with light
- No labeling required

17.9.2 Specifications

Parameter	Typical Value
Axial resolution	1–15 μm
Lateral resolution	10–25 μm
Penetration depth	1–3 mm
A-scan rate	10–400 kHz

17.9.3 OCT Angiography

Contrast from moving blood cells:

- No contrast agent needed
- Capillary-level resolution
- Widely used in ophthalmology

17.10 Comparison of Techniques

Technique	Resolution	Depth	Speed	Invasiveness
Confocal	0.2 μm	0.2 mm	Medium	Requires access
Two-photon	0.5 μm	1 mm	Medium	Requires access
Light-sheet	1 μm	cm	Fast	Cleared samples
PIV/PTV	10 μm	1 mm	Fast	Requires tracers
MRI	0.5 mm	Unlimited	Slow	Non-invasive
Ultrasound	0.1 mm	10 cm	Fast	Non-invasive
OCT	5 μm	2 mm	Fast	Non-invasive

17.11 Computational Image Analysis

17.11.1 Segmentation

Identifying structures:

- Thresholding
- Region growing
- Deep learning (U-Net, etc.)

17.11.2 Tracking

Particle or cell tracking:

- Nearest neighbor linking
- Kalman filtering
- Graph-based optimization

17.11.3 Registration

Aligning images:

- Rigid (translation, rotation)
- Affine (scaling, shearing)
- Deformable (local warping)

17.11.4 Quantification

Extracting measurements:

- Velocity fields from PIV
- Tracer concentration from intensity
- Network morphology (diameter, branching)

17.12 Multi-Modal Integration

17.12.1 Correlative Microscopy

Combining techniques:

- Light + electron microscopy
- Two-photon + electrophysiology
- OCT + fluorescence

17.12.2 Registration Challenges

- Different resolutions
- Different contrast mechanisms
- Tissue deformation
- Coordinate system alignment

17.13 Emerging Technologies

17.13.1 Adaptive Optics

Correcting optical aberrations:

- Wavefront sensing
- Deformable mirrors
- Deeper, sharper imaging

17.13.2 Super-Resolution

Breaking diffraction limit:

- STED, PALM, STORM
- Resolution: 20–50 nm
- Currently limited depth

17.13.3 Photoacoustic Imaging

Light absorption → acoustic waves:

- Combines optical contrast with ultrasound depth
- Endogenous contrast (hemoglobin)
- Resolution: 10–100 μm at cm depth

17.14 Summary

Key Concepts

- **Two-photon microscopy**: Deep tissue imaging (up to 1 mm), reduced photodamage
- **Light-sheet**: Fast volumetric imaging of cleared samples
- **PIV/PTV**: Quantitative flow measurement with tracers
- **MRI**: Non-invasive whole-organ flow, limited resolution
- **OCT**: High-resolution structural imaging to 2 mm depth
- **Trade-offs**: Resolution vs. depth vs. speed vs. invasiveness

17.15 Further Reading

1. Helmchen, F. & Denk, W. (2005). "Deep tissue two-photon microscopy." *Nature Methods*.
2. Stelzer, E.H.K. (2015). "Light-sheet fluorescence microscopy for quantitative biology." *Nature Methods*.
3. Adrian, R.J. & Westerweel, J. (2011). *Particle Image Velocimetry*. Cambridge.
4. Drexler, W. & Fujimoto, J.G. (2015). *Optical Coherence Tomography*. Springer.

Chapter 18

Experimental Gaps and The Prize

18.1 Introduction

This final chapter examines:

- What we cannot yet measure at the mesoscale
- Key unanswered questions in transport biology
- The potential impact of closing these gaps
- Opportunities for computational and experimental advances

18.2 Current Measurement Limitations

18.2.1 Resolution vs. Scale Trade-off

The fundamental challenge:

Requirement	Challenge	Current Status
Cell-level resolution	<10 μm	Achievable in vitro
Tissue-scale FOV	>1 mm	Achievable
Both simultaneously	—	Difficult in vivo
+ Dynamic (real-time)	—	Very difficult
+ Non-invasive	—	Major challenge

18.2.2 In Vivo Flow Measurement Gaps

Perivascular space flow:

- Direct velocity measurements lacking
- Tracer studies show bulk movement, not instantaneous velocity
- Cannot distinguish advection from dispersion
- Gap: Real-time PVS velocity field in living brain

Intestinal mixing:

- Flow near villi poorly characterized
- Unstirred layer thickness debated

- Effect of motility on transport unknown
- Gap: Simultaneous flow and concentration measurement

18.2.3 Mechanical Property Measurement

Tissue stiffness in situ:

- MR elastography: mm resolution
- AFM: requires access, local
- Gap: Non-invasive, high-resolution tissue mechanics

18.2.4 Molecular Concentration Gradients

In living tissue:

- Oxygen: phosphorescent probes, limited depth
- Metabolites: sensors immature
- Signaling molecules: low concentrations, dynamic
- Gap: Multiplexed, real-time molecular imaging

18.3 Key Unanswered Questions

18.3.1 Glymphatic System

1. **What drives PVS flow?**
    - Relative contribution of cardiac vs. vasomotion vs. respiration
    - Direction and magnitude of flow
    - Regional variations
2. **How do solutes cross parenchyma?**
    - Bulk flow vs. diffusion/dispersion
    - Role of ISF space changes
    - Pathway through tissue
3. **Why does sleep enhance clearance?**
    - Mechanistic basis
    - Which sleep stage most effective
    - Can it be enhanced pharmacologically
4. **How does aging impair the system?**
    - Which component fails first
    - Reversibility
    - Intervention targets

18.3.2 Intestinal Transport

1. **What is the true UWL thickness?**
    - Varies by technique and condition
    - Dynamic during digestion
    - Effect on absorption kinetics
2. **How does villus motility affect absorption?**
    - Quantitative enhancement factor
    - Optimal motion patterns
    - Failure in disease
3. **What causes pathological gas accumulation?**
    - Production vs. absorption imbalance
    - Trapping mechanisms
    - Role in infant colic, NEC

18.3.3 Vascular Transport

1. **How does microvascular heterogeneity affect delivery?**
    - Network-level flow distribution
    - Temporal fluctuations
    - Impact on drug delivery
2. **What controls angiogenesis patterning?**
    - Rules for branching decisions
    - Achieving Murray's law
    - Why tumors fail

18.4 The Prize: Disease Impact

18.4.1 Neurodegenerative Disease

Alzheimer's disease:

- 6+ million patients in US
- $350 billion annual cost
- No disease-modifying therapy

If we understood glymphatic clearance:

- Early detection of impairment
- Sleep-based interventions
- Drug targets for enhancement
- Prevention strategies

Parkinson's disease:

- 1+ million in US
- α-synuclein spread via glymphatics?
- Similar intervention potential

18.4.2 Neonatal Disease

Necrotizing enterocolitis:

- Leading cause of neonatal surgical death
- 10,000+ cases/year in US
- 20–30% mortality

Understanding mesoscale transport could enable:

- Predictive biomarkers
- Feeding optimization
- Intervention timing

Infant colic:

- Affects 10–30% of infants
- Significant family distress
- Unknown etiology

Potential insights:

- Gas dynamics understanding
- Motility pattern optimization
- Targeted interventions

18.4.3 Cardiovascular Disease

Atherosclerosis:

- #1 cause of death globally
- Shear stress patterns predict plaque location

Better mesoscale models could:

- Identify high-risk anatomy
- Optimize stent design
- Guide surgical planning

18.4.4 Cancer

Drug delivery:

- Most drugs don't reach tumor interior
- Heterogeneous vasculature
- High interstitial pressure

Understanding tumor mesoscale transport enables:

- Optimized dosing schedules
- Vascular normalization strategies
- Combination therapy timing

18.5 Quantifying the Prize

18.5.1 Healthcare Impact

Disease	Annual Cost (US)	Potential Reduction
Alzheimer's	\$350 billion	10–30%
Heart disease	\$230 billion	5–15%
Cancer	\$200 billion	5–20%
GI diseases	\$140 billion	10–20%

Even modest improvements represent billions in savings and improved quality of life.

18.5.2 Quality of Life

Beyond economics:

- Cognitive preservation in aging
- Reduced infant suffering
- Better cancer outcomes
- Personalized medicine

18.6 Bio-Inspired Engineering

18.6.1 Learning from Biology

Biological systems have optimized:

- Transport networks (Murray's law)
- Heat exchangers (countercurrent)
- Mixing (villus motion, cilia)
- Self-organization (angiogenesis)

18.6.2 Engineering Applications

Microfluidic design:

- Murray's law channel networks
- Uniform distribution manifolds
- Optimal mixing geometries

Heat exchangers:

- Tree-shaped cooling networks
- Constructal design principles
- Electronics cooling

Chemical reactors:

- Hierarchical porous catalysts
- Optimal mass transfer
- Liver-inspired bioreactors

Tissue engineering:

- Pre-vascularized scaffolds
- Oxygen delivery optimization
- Organ preservation

18.7 Computational Opportunities

18.7.1 What Models Can Provide

- Test hypotheses before experiments
- Interpolate between measurements
- Explore parameter space
- Predict system behavior
- Guide experimental design

18.7.2 Current Limitations

- Validation data lacking
- Multi-scale coupling challenging
- Computational cost for 3D, dynamic
- Parameter uncertainty

18.7.3 Opportunities for MesoBio

The framework can address:

- GPU-accelerated LBM for real-time flow
- Agent-based cells with mechanotransduction
- Coupled transport and reaction
- Multi-physics integration

18.8 Future Directions

18.8.1 Experimental Advances Needed

1. **Non-invasive flow imaging**
    - Improved MRI resolution/speed
    - Functional ultrasound advances
    - New contrast mechanisms
2. **Molecular sensors**
    - Genetically encoded reporters
    - Implantable sensors
    - Non-invasive metabolic imaging
3. **Organ-on-chip integration**
    - Standardization
    - Improved physiological relevance
    - Validated models

18.8.2 Computational Advances Needed

1. **Multi-scale methods**
    - Seamless molecular-to-tissue coupling
    - Adaptive resolution
    - Uncertainty propagation
2. **Machine learning integration**
    - Physics-informed neural networks
    - Surrogate models for speed
    - Image analysis automation
3. **Personalized models**
    - Patient-specific geometry
    - Individual parameter estimation
    - Real-time clinical decision support

18.8.3 Collaboration Needs

Closing mesoscale gaps requires:

- Experimentalists + modelers
- Biologists + engineers + clinicians
- Academia + industry + regulators
- Open data and code sharing

18.9 Call to Action

18.9.1 For Experimentalists

- Design experiments with modeling in mind
- Report all parameters (not just "interesting" results)
- Share raw data
- Engage with modelers early

18.9.2 For Modelers

- Validate rigorously
- Quantify uncertainty
- Make predictions that can be tested
- Make code available

18.9.3 For Clinicians

- Identify unmet needs
- Provide clinical context
- Participate in translational research
- Champion new technologies

18.10 Conclusion

The mesoscale represents a critical frontier in biology:

- Where cellular behavior becomes tissue function
- Where transport physics determines outcomes
- Where intervention can have greatest impact

The tools are maturing:

- Imaging at increasing resolution and depth
- Organ-on-chip for controlled studies

- Computational methods for multi-physics
- GPU acceleration for practical simulation

The prize is substantial:

- Understanding disease mechanisms
- Developing targeted therapies
- Improving human health
- Inspiring new engineering

The mesoscale awaits exploration.

18.11 Summary

Key Takeaways

- **Measurement gaps**: Cannot yet achieve cell resolution + tissue scale + real-time + non-invasive
- **Key questions**: Glymphatic drivers, intestinal mixing, vascular heterogeneity
- **Disease impact**: Neurodegeneration, neonatal disease, cardiovascular, cancer
- **Engineering opportunities**: Bio-inspired design based on biological optimization
- **Path forward**: Integration of experiments, computation, and clinical translation

18.12 Final Thoughts

The mesoscale is where biology becomes engineering and where physics constrains life. Understanding this scale—through rigorous experiment, validated computation, and clinical translation—offers the potential to transform medicine and inspire technology.

The MesoBio framework aims to be one tool among many in this endeavor. We hope this guide has provided the conceptual foundation for computational scientists entering this exciting field.

"The important thing in science is not so much to obtain new facts as to discover new ways of thinking about them."
—William Lawrence Bragg

Quick Reference

Key Dimensionless Numbers

Number	Formula	Range	Interpretation
Reynolds	$\mathrm{Re} = UL/\nu$	10^{-3} – 10^{2}	Inertia vs. viscosity
Peclet	$\mathrm{Pe} = UL/D$	10 – 10^{4}	Advection vs. diffusion
Womersley	$\mathrm{Wo} = R\sqrt{\omega/\nu}$	0.1 – 10	Pulsatility effects
Damköhler	$\mathrm{Da} = \tau_{\mathrm{flow}}/\tau_{\mathrm{rxn}}$	0.1 – 100	Reaction vs. transport
Darcy	$\mathrm{Da} = K/L^2$	10^{-6} – 10^{-2}	Porous media resistance

Key Governing Equations

Equation	Application
$\rho\left(\frac{\partial \mathbf{u}}{\partial t} + \mathbf{u}\cdot\nabla\mathbf{u}\right) = -\nabla p + \nabla\cdot\boldsymbol{\tau} + \mathbf{f}$	Navier-Stokes
$\frac{\partial C}{\partial t} + \mathbf{u}\cdot\nabla C = D\nabla^2 C + R$	Advection-diffusion-reaction
$P_{\mathrm{open}} = \frac{1}{1+\exp\left(-k(\sigma-\sigma_{1/2})\right)}$	Piezo channel gating
$r_0^3 = r_1^3 + r_2^3$	Murray's Law (vascular)
$\sigma = \sum_i J_i X_i \geq 0$	Entropy production

Biological Length and Time Scales

Structure/Process	Scale	Key Physics
Mitochondrial cristae	20–50 nm	Proton gradients
Single cell	10–30 μm	Agent-based modeling
Intestinal villus	0.5–1.5 mm	Mass transfer
Liver lobule	1–2 mm	Perfusion zones
Perivascular space	20–100 μm	Glymphatic flow
Cardiac cycle	$\sim$1 s	Pulsatile flow
Cell division	$\sim$24 h	Phenotype changes
Glymphatic clearance (sleep)	6–8 h	Waste removal

MesoBio Framework Quick Start

```
# Simulate CSF flow in perivascular space
import jax.numpy as jnp
from mesobio.solvers.fluid.lbm import D2Q9Solver
from mesobio.backends import JAXBackend
```

```
# Initialize backend and solver
backend = JAXBackend()
solver = D2Q9Solver(
    nx=200, ny=80,
    viscosity=0.697e-6,  # CSF viscosity (m^2/s)
    backend=backend
)

# Set pulsatile boundary condition
def cardiac_wall(t):
    return A * jnp.sin(2 * jnp.pi * f_heart * t)

# Run simulation
for step in range(n_steps):
    solver.step(wall_velocity=cardiac_wall(t))
    if step % save_interval == 0:
        velocity = solver.get_velocity()
        save_field(velocity, step)
```

Key References

1. Schrödinger, E. (1944). *What is Life?* Cambridge University Press.
2. Lane, N. (2015). *The Vital Question.* W.W. Norton.
3. Bejan, A. (2016). *The Physics of Life.* St. Martin's Press.
4. Fung, Y.C. (1993). *Biomechanics.* Springer.
5. Succi, S. (2018). *The Lattice Boltzmann Equation.* Oxford.
6. Iliff et al. (2012). "A paravascular pathway facilitates CSF flow." *Sci Transl Med.*
7. Mestre et al. (2018). "CSF flow is driven by arterial pulsations." *Nat Commun.*
8. Ingber, D.E. (2016). "Reverse engineering human pathophysiology with organs-on-chips." *Cell.*